Summer 2012

Analysis of Mechanically Milled Exchange Coupled Nanocomposite Permanent Magnets

Santanu Mukherjee
University of Nebraska-Lincoln, santanu.mukherjee@huskers.unl.edu

Analysis of Mechanically Milled Exchange Coupled Nanocomposite Permanent Magnets

by

Santanu Mukherjee

A THESIS

Presented to the Faculty of

The Graduate College at the University of Nebraska

In Partial Fulfillment of Requirements

For The Degree of Master of Science

Major: Mechanical Engineering

Under the Supervision of Jeffrey E. Shield

Lincoln, Nebraska

May, 2011

Analysis of Mechanically Milled Exchange

Coupled Nanocomposite Permanent Magnets

Santanu Mukherjee

University of Nebraska, 2012

Advisor: Jeffrey E. Shield

Nanocomposite permanent magnets have recently evoked wide interest because of their interesting properties. They usually consist of a hard magnetic phase having superior coercivities and a soft magnetic phase having improved values of magnetization and when they are coupled together, we get a permanent magnet with enhanced values of both the parameters and thus can be put to a lot of applications. Also to make this possible we can take advantage of the principle of exchange interaction which has been discussed subsequently in detail.

Also the microstructure plays a major role in obtaining good magnetic properties and the microstructure is usually controlled by the cooling rates i.e. the wheel speeds during the melt spinning process as well as heat treatment process i.e. annealing. Both these experimental techniques have been used to study the variation of magnetic properties of $Nd_{12}Fe_{82}B_6$ and $Nd_{10}Fe_{84}B_6$ which were formed using different wheel speeds. They were also annealed to study the changes in their magnetic properties. Mechanical milling was employed to improve the coercivities of the as cast system.

The next project was to build a non-rare earth permanent magnet using MnIr-Fe. Mechanical milling and subsequent annealing was used to study the changes in phase and the subsequent improvement in magnetic properties. The principle behind this was the exchange coupling of the antiferromagnetic MnIr alloy with the soft ferromagnetic Iron.

ACKNOWLEDGEMENTS

Firstly, I would like to take this opportunity to express my deep sense of gratitude to my advisor, Dr. Jeffrey E. Shield for the wonderful way in which he has guided me through my research. He has always been patiently available whenever I have had questions and has motivated me to perform to my best. His encouragement has been the very helpful to me for the completion of this thesis.

I would also like to take this opportunity to thank the members of my research group for their continuous support and help. Their cooperation was extremely kind and helpful. I am deeply thankful to Dr. Jayaraman, Farhad, Mak, Hellen, and Pinaki for taking time out from their busy schedules to help me out whenever I needed.

Lastly, I must express my deepest regards to my family for constantly being beside me, and my friend who helped me to finish my work.

TABLE OF CONTENTS:

1. INTRODUCTION & OBJECTIVES

1.1 BACKGROUND:

Magnets have been known to man since ancient times, the mineral Magnetite (Fe_3O_4) was the first of such. It was called the “lodestone” and was used as a crude compass for direction finding. Since then the science of magnetism and the research on newer and better permanent magnetic materials have come a long way and in today's world the use of magnets is ubiquitous including applications in computer hard drives for memory, motors in cars, in various space applications, in speakers and microphones and medical uses.

1.2 MAGNETIC MATERIALS AND THEIR PROPERTIES:

Most common magnetic materials can be classified as having diamagnetic, paramagnetic and ferromagnetic properties. A diamagnetic material is one which actually repels the applied magnetic field. A paramagnetic material tends to align itself towards an applied magnetic field and has a small positive susceptibility, but rapidly loses its magnetization as soon as the applied field is removed.

1.2.1 Origins of Magnetism:

Magnetism is an important phenomenon that originates at the atomic level. In an atom there are many electrons and these are revolving in their respective orbits around the nucleus as well as spinning around in their own axes. Both of these kinds of motion gives rise to magnetic moments and these moments are vector quantities. These moments are so aligned that they are in the direction of the spin axis and perpendicular to the axis of revolution around the orbit [1]. Thus, the net magnetic moment of an atom has three fundamental contributions: the electronic spin which is a fundamental property of the

electron itself, the angular moment generated due to its revolution and a change in the orbital angular moment due to an externally applied magnetic field. These can give rise to fundamentally two different conditions.

(i) All the magnetic moments are random and they vectorially nullify each other. There is no resultant magnetic moment and this situation is called diamagnetism.

(ii) On the other hand, there might be a net resultant magnetic moment as the moments do not cancel each other out and therefore the atom has a net moment. It can be paramagnetic, ferromagnetic or antiferromagnetic depending on the strength of the resultant moment and the orientation of the spins [1, 2].

A **paramagnetic** material is one that has a random arrangement of atomic spins. As a result in the absence of an external magnetic field, the spins cancel each other out and there is no net magnetization. However, when an external field is applied the spins tend to align themselves with the direction of the external field and a small net magnetization is obtained. The random arrangement of the spins in a paramagnetic material in the absence of an applied magnetic field is shown schematically in Figure 1.1.

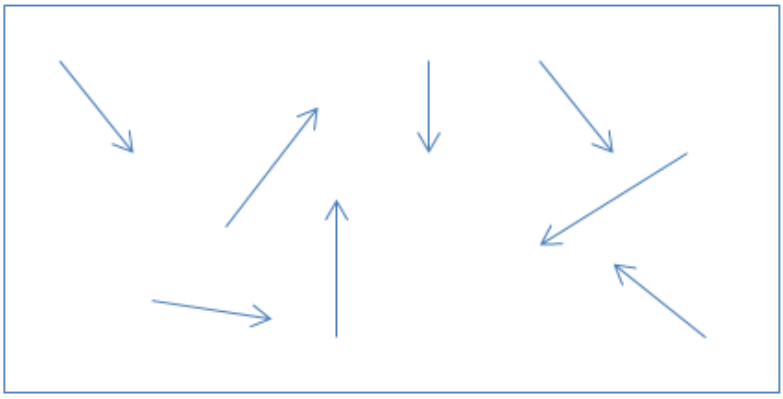

Figure 1.1: *This represents the random arrangement of spins in a domain of a paramagnetic material in the absence of an externally applied magnetic field.*

A **ferromagnetic** material exhibits certain characteristics by which we are able to characterize them both qualitatively and quantitatively, and it is these properties that make it suitable for so many applications. At a fundamental atomic level, it has been understood that in a domain for a ferromagnetic material, the spins are aligned in the same direction even without an external magnetic field. This can be represented by the schematic diagram shown in Figure 1.2.

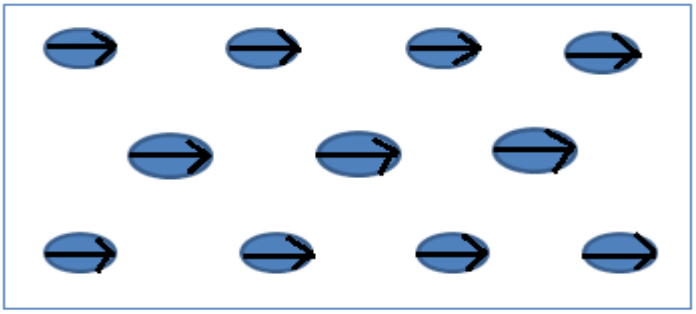

Figure 1.2: *This represents the parallel alignment of spins in a ferromagnetic domain.*

The most important of these properties that we have to consider are the magnetization (M), the remanence (Br) and coercivity (Hc). All these quantities can be obtained from the hysteresis curve from magnetic measurements of the sample and are a characteristic of most ferromagnetic materials. On the application of a magnetic field (H) to a non-magnetized ferromagnetic material (Figure 1.3), the microscopic randomly oriented magnetic domains inside it gradually tend to align with the applied field and the magnetization (M) increases. This goes on until a maximum value of M is reached, which is when all the magnetic domains inside the material are in the direction of the applied field and further increase of H will have no effect on M. This value is called the saturation magnetization (M_s). When the direction of the applied field is reversed, each microscopic magnetic domain inside the material tend to reverse and start aligning itself with the

direction of the reversed field, and consequently, it does not follow the same trajectory as when it was being initially magnetized. In this case we notice that the there is some amount of magnetization remaining when H is zero, this is called the remanence (M_r). Further reversal of H results in the magnetization coming to a zero value, that is, all the internal magnetic domains are now randomly arranged and there is no net magnetization. This value is called coercivity (H_c) and can be a measure of how strong the magnet is and its ability to withstand a demagnetizing field. The saturation can be reached even in this negative field direction and therefore this produces a hysteresis loop which is characteristic of ferromagnetic materials.

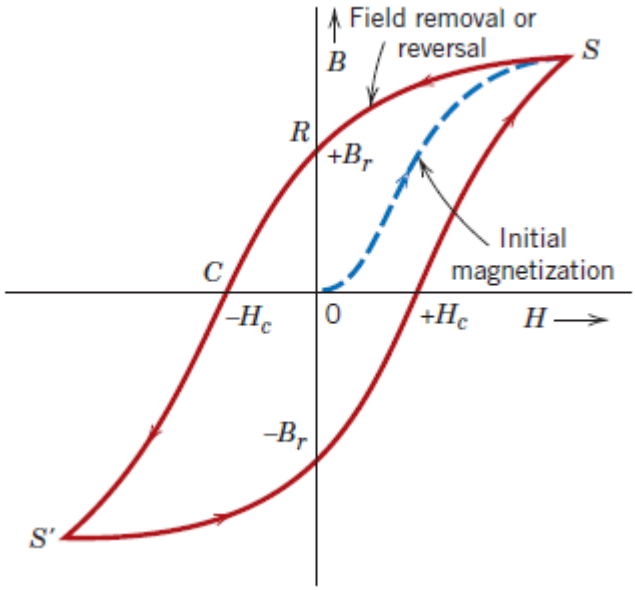

Figure 1.3 *A typical hysteresis loop of a ferromagnetic material.* [3]

On the other hand, an **antiferromagnetic material** is one that exhibits antiparallel alignment of spins between the adjacent atomic layers. It is understood from this type of arrangement that the opposite spins cancel each other out and hence there is no net magnetization in the bulk material. The schematic arrangement of the spin orientation in an antiferromagnetic domain is shown in Figure 1.4.

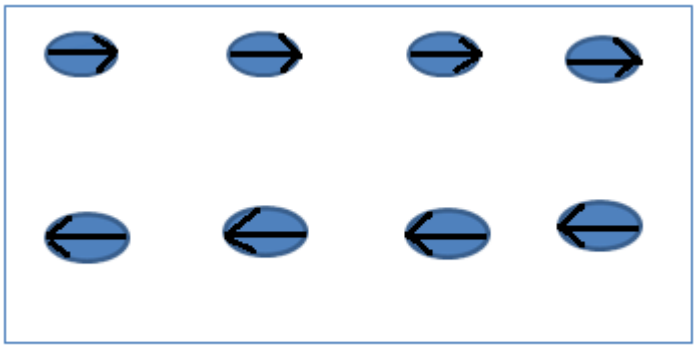

Figure 1.4: *This represents the antiparallel arrangement of spins between adjacent atomic layers in an anti-ferromagnetic domain.*

1.3 ALLOYS, PHASES AND PHASE DIAGRAMS:

Alloys are very important materials from a metallurgical point of view. They are used widely and their necessity and usage both has far reaching engineering and structural applications. Steel is a well-known and commonly used alloy, containing iron and carbon as its main constituents, and it is used in various structural applications. Pure elemental metals have certain drawbacks which make them unsuitable for use in their elemental form. Therefore other elements have to be added in certain amounts which tend to enhance their properties and this process is called alloying, and the resultant material so obtained is an alloy. The alloys are almost always formed to enhance certain physical properties such as strength, ductility, corrosion resistance properties and ability to withstand stress and fatigue [4, 5].

The arrangement of atoms in the alloys is responsible for its crystal structure and the way this arrangement changes from the parent metal is what gives the resulting alloy its particular characteristics. There are three types of possible ways in which we can find a

suitable model of the atomic and crystallographic arrangement in alloys. They can be enumerated as below:

(i) Solid Solution: In this system the alloying components dissolve in each other, hence they are called a solid solution. This is similar to a liquid solution in the fact that the resultant alloy is homogenous in composition throughout, provided thermodynamic equilibrium is maintained. Usually the parent crystal structure of the solid solution is the lattice structure of the solvent, and it is understood that solvent atoms either substitute for or migrate to interstices in the lattice of the solvent, depending on which it can be further classified as a substitutional solid solution or an interstitial solid solution [3, 4]. The lattice site chosen for substitution is totally random and this is called a disordered solid solution; however the factors that play a major role in the formation of these solid solutions are that: the solute and solvent atoms should have similar electronic electronegativity, similar crystalline nature and similar size. Collectively these empirical rules, also called the Hume-Rothery Rules lay down a criterion for the formation of substitutional solid solutions [4, 5]. If however, there are fixed preferences for the solvent atom to attach to particular lattice sites then the resulting substitutional solid solution is called ordered.:

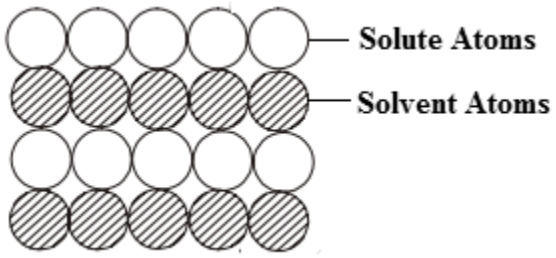

Figure 1.5: *The above figure represents the arrangement of atoms in an ordered substitutional solid solution* [3].

However, instead of the above arrangement if solvent atom is migrating to intermediate position in the lattice, that is, where there are interstitial sites (i.e. where the atoms should

not be), then such a solid solution is called an interstitial solid solution. The interstitial solute atom must be relatively smaller in size so that it can be accommodated in the void. Common interstitial atoms may be carbon or nitrogen. For example, the γ-Fe has a FCC crystal structure i.e. they are at the corner and face center points and C interstitial atoms migrate to the body center or the edge centers where they can be accommodated [3]. An interstitial solid solution can be represented by a schematic arrangement as shown below:

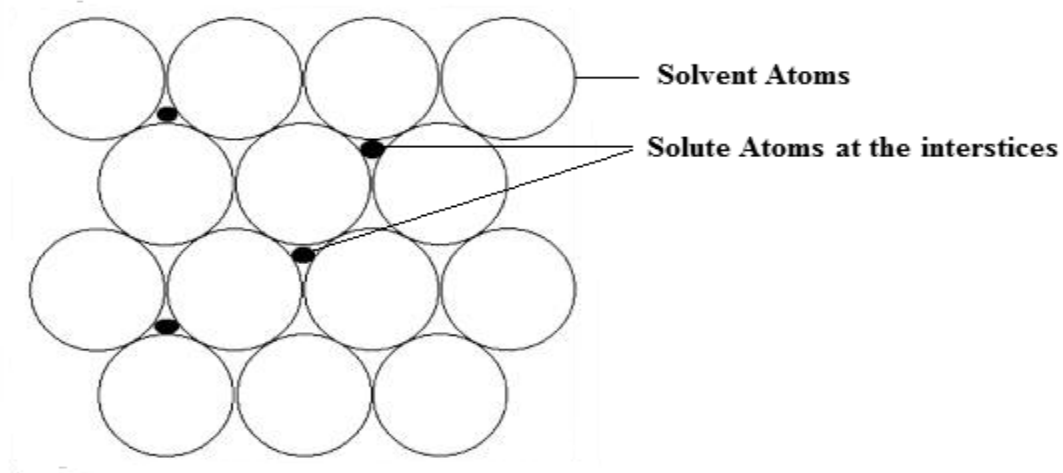

Figure 1.6: *This represents a schematic arrangement of an interstitial solid solution* [3, 4].

(ii) Chemical Compounds: Chemical compounds are when the combining metallic elements undergo a reaction and the net electronic arrangement totally changes to form a compound i.e. the crystal structure of the newly formed alloy is entirely different from the parent metals. They may be ionic compounds formed between atoms of differing electronegativities, electron compounds formed between metals having high melting points and low melting points and also interstitial metallic alloys which are formed between metals having higher melting points and crystallizing in the cubic system with metalloids having a lesser atomic radius [3, 4].

On the other hand, there may be covalent compounds formed by covalent bonding. This arises when there is a sharing of electron pairs between two atoms. This type of bonding is usually seen in atoms that exhibit very similar electronegativities e.g. H_2, O_2, CH_4, CO_2 to name a few.

(iii) Eutectic: An eutectic can be defined as a mixture of two phases which have crystallized from a molten solution. The temperature at which this eutectic formation takes place is usually the lowest melting point in the entire system. It has been observed that the constituents of a eutectic may be solid solutions or even elemental metals themselves. The iron-carbon alloys exhibit a eutectic microstructure. The ductility and the rigidity of the resultant eutectic alloy are a function of the ductility and the rigidity of the combining phases respectively. Eutectic alloys of Sn and Pb are extensively used for soldering in various industrial applications [4].

Instead of the alloy developing from the liquid phase, if it so happens that the alloy develops in two distinct phases from another solid itself then such a transformation is called eutectoid and the resultant alloy is an eutectoid alloy. This is commonly observed in the Iron-Carbon system, in which the austenite phase transforms to ferrite and cementite at 1050C approximately.

It is seen that that alloys and the way they are formed play a very important role in the properties it exhibits. The crystallographic arrangement of the alloys is therefore very important as they play the major role in deciding how the properties of it will be. Another important consideration to be kept in mind is that the combining elements in the alloy also play a major role in determining the resultant crystallographic arrangement of the alloy based on their own respective atomic structures, as we saw in the Hume-Rothery rules. The phase diagram of an eutectic system can be as shown below:

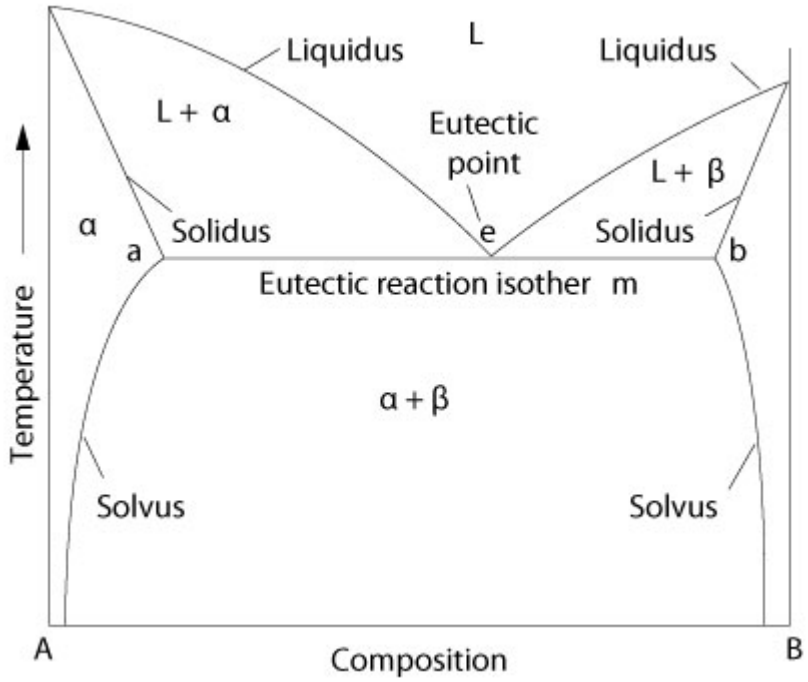

Figure 1.7: R*epresentation of the phase diagram of a typical eutectic system* [4].

1.4. $L1_0$ CRYSTAL STRUCTURE:

There are many ordered crystalline structures. One among them is the $L1_0$ crystals, which exhibit ordering. They can be considered to be an ordered derivative from the parent FCC structure [6]. The equiatomic alloy MnIr forms this type of crystal structure.

Therefore in the $L1_0$ structure, we can say that the instead of the equal probability of finding an Mn or an Ir atom in the equiatomic FCC atomic arrangement, there is a definite atomic arrangement of the two types of atoms. The two distinct types of crystallographic arrangements can be showed in the given figure.

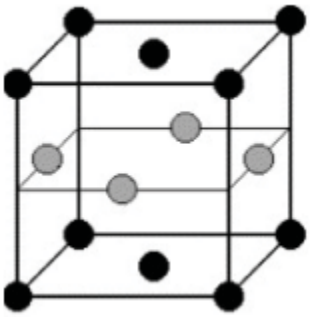

Different type of atoms at another face center

identical atoms at corners two pairs of face centers.

Figure 1.8: *This represents a schematic arrangement of atoms in an L10 crystal structure* [6].

As mentioned above, in the FCC structure the same type of atoms occupies the lattice sites or if it is an alloy there will be an equal probability of finding the different types of atoms at a particular lattice position. However, this is not the case of the L10 structure. In this case for an alloy, the lattice sites in two faces are occupied by one type of atoms and the second type of atoms are present at the lattice sites of the corner and the other face. It is to be understood that such a structure has a reduced symmetry with respect to its parent structure. The prototype phase for the L10 structure is the CuAuI structure. There are eight opposite near neighbors and four similar near neighbors as can be seen from the structure in Figure 1.8 [6, 7].

MnIr forms a $L1_0$ and in this case exhibits antiferromagnetic behavior, according to the alignment of the electronic spins. Another major advantage that these crystals tend to have a higher value of the Nêel temperature, which means that they can be suitable used for high temperature applications. The Neel temperature of the MnIr antiferromagnetic crystal is approximately 1100K [8].

Because of this antiferromagnetic behavior, such materials can be widely used in thin films for high density recording media. They can also be exchange coupled with ferromagnetic materials to form nanocomposite permanent magnets which also has a lot of varying applications.

1.4 EXCHANGE INTERACTION:

Exchange interaction or exchange coupling is a very important phenomenon that we must consider when we consider the case of nanocomposite magnets. Exchange interaction is primarily a quantum mechanical phenomenon with no classical analogue. Just as there is repulsion between like charges and attraction between unlike charges, this type of interaction mainly takes into consideration a two-atom system. This exchange interaction depends on the spin states of the respective atoms and based on the Pauli's exclusion principle which requires that no two electrons in a same system can have identical values of all four quantum numbers. If the values of the other quantum numbers are the same, then the spin quantum number value will be different. Therefore if even the spins are to be in the same direction, i.e. parallel then the system will have a higher value of energy, the electrons will repel each other and the system will be unstable. On the other hand, antiparallel spin states result in reduced energy and the system is more stable in that case.

If the system is considered as consisting of two adjacent atoms i and j, then the term "exchange" originates because not only do the electrons revolve around their own orbits, also the electron from the i^{th} atom revolves around the nucleus in the j^{th} atom and vice versa. Therefore we can say that another term, i.e. the "exchange energy" term can be used to indicate this type of interaction, because fundamentally what is taking place is an exchange or interchange of electrons between the two adjacent atoms, which results in a kind of interaction. This can be mathematically put in by the equation as:

$$Eex = - 2J_{ex}. S_i. S_j. \cos \varphi$$

The terms S_i and S_j can be thought to be the spin states of the two adjacent atoms i and j and φ is the angle between the two exchange interacting spin states. Also J_{ex} is called the exchange integral and this is the fundamental parameter which is most important in this case [1].

From this equation, it is seen that the condition of minimum energy of the system is when the spins are parallel ($\varphi = 0$ or $\cos \varphi = 1$). For a negative value of exchange integral, the condition of stability reverses, i.e. the stability is obtained when the spins are antiparallel. With respect to permanent magnets, it is understood that all the spins being oriented in the same direction should be the most stable condition and therefore J_{ex} is positive [1].

However, this is a special condition and therefore there are certain factors attached to it. Now to consider a multi-atom system such that the net spins will be parallel because of these exchange forces when they are separated by a certain distance. If they come in close proximity to each other and behave for all intents and purposes like a single atom system, then for stability antiparallel spins will be preferred. Therefore there is a distance for which exchange interaction is preferred and below which, the Pauli repulsion comes into the picture. Exchange interaction is a very powerful phenomenon which is responsible for improving the magnetic properties in nanocomposite permanent magnets [1]. Therefore we see that the exchange interaction is a parameter that is very fundamental and is responsible for controlling the magnetic properties at an atomic level. Exchange coupling is commonly the technique used to enhance the magnetic properties of nanocomposite permanent magnets, where a magnetically hard phase (having higher coercivity) is coupled with a magnetically soft phase (having higher magnetization) resulting in the product having enhanced values of both the parameters.

1.6. NANOCOMPOSITES:

The basic idea of nanocomposites comes from the very early idea of mixing or combining two or more different materials to get enhanced and superior properties of the resultant product. This could be due to some interaction between the combining materials which results in superior properties. A nanocomposite can also be considered to be a solid which

has multiple phases. The size of the individual grains should usually be less than 80-100 nm. Also it is interesting to note that nanocomposites are not always something that has been engineered or man-made, they are also naturally found, and for example the structure of the bone is in the form of a nanocomposite of bone mineral, compact bone tissue, nerve endings and organic matter such as collagen [9].

Nanocomposite permanent magnets also have started to attract a lot of attention recently because of their promising characteristics. The theoretical concept of these types of magnets was proposed by Kneller and Hawig [10], while the first experimental evidence of two-phase nanocomposite permanent magnets displaying “exchange-spring” behavior was reported by Coehoorn, et al. [11]. Hadjipanayis provided a summary of materials and processes [12]. In many instances, the hard magnetic phase is based on the $R_2Fe_{14}B$ compound, while the magnetically soft phase is Fe or Fe3B. Nanostructuring has been effectively accomplished by rapid solidification, crystallization of amorphous precursors, or mechanical milling/alloying. We can consider the principles of exchange interaction as well as exchange biasing to understand the enhanced properties of nanocomposite permanent magnets.

Exchange coupling is an important phenomena observed in nanocomposites. It is responsible for greatly enhancing the magnetic properties. It is a principle by which when a soft and a hard magnetic phase are brought in intimate contact a higher energy product is expected and also enhanced remanence [13]. Theoretical calculations predict that an energy product of approximately 50 MGOe or even greater can be reached for isotropic materials, but actually about 10-20 MGOe is obtained [14, 15]. This discrepancy is usually due to the inability of controlling the microstructure to obtain the optimum magnetic properties. Also lack of proper anisotropy is another reason why the full potential of the energy product is not achieved. Various techniques have been used to overcome these

drawbacks. Chang et al have used La and Cr to dilute the rare earth component and have shown an increase in the energy product value [14]. Mechanical alloying and subsequent heat treatment was studied by various research groups also, for the case of Nd-Fe-B nanocomposite permanent magnets. McCormick et al. has achieved a coercivity of approximately 5.2 kOe for mechanically milled and subsequently annealed $Nd_{10}Fe_{84}B_6$ samples [17]. Mechanical milling tends to increase the intimate contact between the soft and the hard phase and thereby improving the exchange interaction [9, 14].

Exchange biasing is another type of phenomena which tends to enhance the properties of nanocomposite permanent magnets. When there are two different phases i.e. an antiferromagnetic phase (AFM) in close contact with a ferromagnetic phase (FM), and this particular interface is cooled through the Neel temperature, an exchange bias is introduced [18]. This type of anisotropy is widely utilized in various applications like recording media, recording heads, etc. The phenomena can be understood as the movement of the AFM spins with the FM spins when an external field is applied. A small torque is exerted on the FM spins by the AFM spins when they tend to rotate along with the change of direction of the AFM spins and this has to be overcome, which gives rise to the anisotropy. The FM spins therefore can be said to have only one easy direction of magnetization, when they are aligned in the same direction as the spins of the AFM layer closest to the interface. Therefore there is unidirectional anisotropy in the exchange biased system [18]. This also results in a shift of the hysteresis loop.

Exchange bias systems have been widely utilized and studied. Mechanical Milling has been employed to study this type of anisotropy. One system that has been studied is the Fe,Ni/CoO system as the FM-AFM phases respectively. It was noticed that a maximum coercivity was obtained after about 30 hours of milling the sample taken in 1:1 ratio [15]. Another system that has been studied is the FeCo-MnO nanocomposites. Milling was done

up to 150 hours in this case to study the effects of exchange bias. It was seen that there was a considerable improvement in the squareness of the hysteresis loop and consequently the coercivity. Exchange bias as well as defects introduced due to the milling are responsible for this. Exchange bias has also been studied extensively in the SmCo-NiO system also. $SmCo_5$ was mixed with NiO and ball milling was done for extended periods. It was noticed that there was a significant increase in peak width indicating development of strain within the crystallites. An increase in coercivity is however noted with the increase in milling times [17]. Exchange bias mainly occurs due to the anisotropy at the interface of the AFM-FM layers. Nanostructures are necessary as a better exchange biasing will occur if the two phases are mixed intimately in nanoscale dimensions.

1.6.1 Neodymium-Iron-Boron Nanocomposite Permanent Magnets: Neodymium-Iron-Boron (Nd-Fe-B) permanent magnets are the best known permanent magnets used in various applications today. They have a wide variety of applications from medical appliances, hard drives and disks, automobile applications, consumer and office electronics and almost all applications which need a strong and reliable permanent magnet. Nd-Fe-B permanent magnets are usually nanocomposites that contain a magnetically hard phase: $Nd_2Fe_{14}B$ (the "2-14-1 phase") that has a high coercivity exchange coupled with soft phase, the α-Fe phase. Credit for discovering the $Nd_2Fe_{14}B$ phase goes to Sumitomo Special Metals in Japan and simultaneously by General Motors in the US in 1982. Since then the use of this type of magnet has increased by large numbers [15].

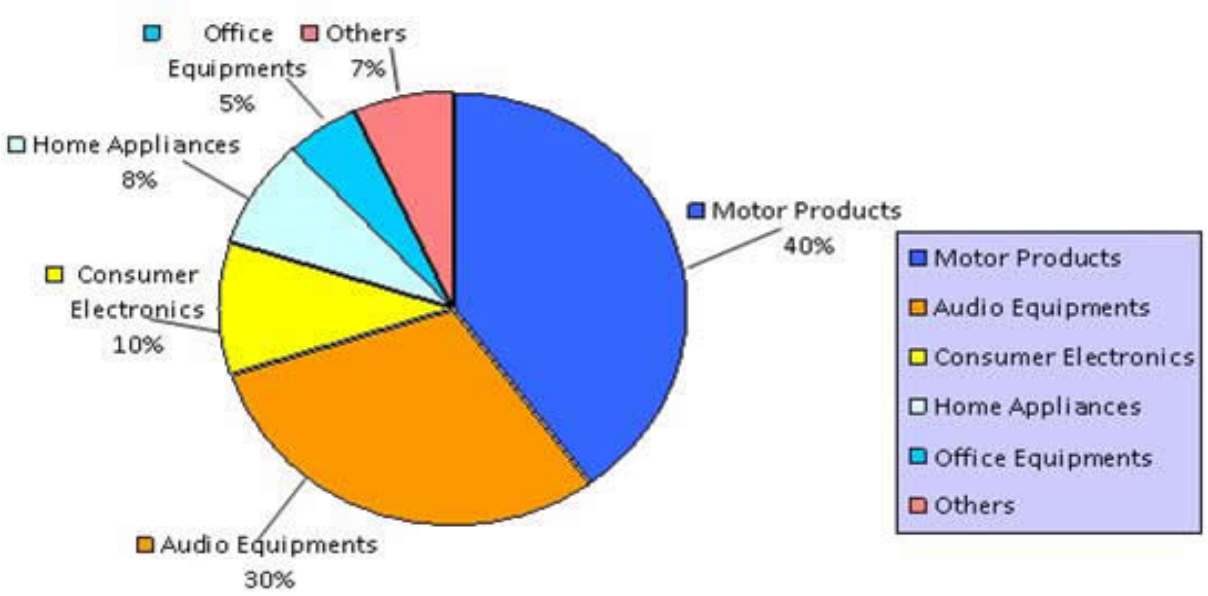

Figure 1.9: *This represents a pie-chart of the percentage utilization of Nd-Fe-B permanent magnets in various industries.* (**Courtesy**: China Rare Earth Magnet Ltd.)

Extensive studies on Nd-Fe-B nanocomposite permanent magnets have been done. They usually consist of the $Nd_2Fe_{14}B$ phase and the α-Fe phase. In this system, the $Nd_2Fe_{14}B$ is the magnetically hard phase and the α-Fe is the soft magnetic phase. It is understood that for exchange coupling to effectively occur, there should be a degree of homogeneity of the grains and they must also be intimately in contact with each other. There have been reports also that there is an increase in the remanence ratio due to the exchange coupling, however other factors can also contribute to the remanence enhancement, for example dipolar coupling. [15, 16] These nanocomposites are usually prepared by rapid solidification techniques, for example melt spinning, which tends to produce a good nano-crystalline structure. The pseudo binary phase diagram of the system is shown in Figure 1.10.

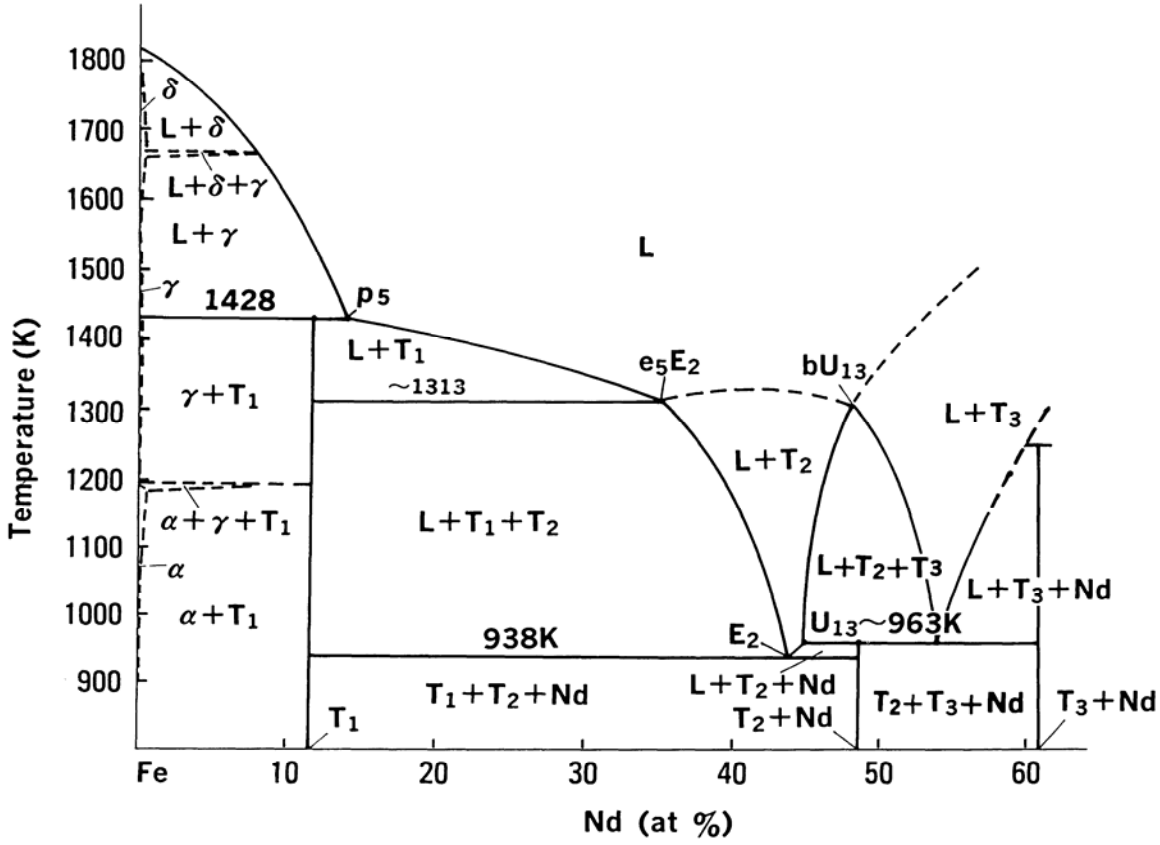

Figure 1.10 *The pseudo binary phase diagram of the Nd-Fe-B ternary system* [10]

Structurally $Nd_2Fe_{14}B$ exhibits a tetragonal structure with the space group being P42/mnm [14, 15]. It has been reported that it usually exhibits a structure which is layered and there is an alternating sequence of stacking of one Nd rich layer and Fe sheet. This tetragonal structure is a major contributor to the fact that the Nd-Fe-B magnets have a high value of the uniaxial magnetocrystalline anisotropy [15].

The major advantages of the Nd-Fe-B are that they usually show a high remanence and a high energy product. Their coercivities are high and they also have a low processing cost. They can be produced industrially by usually two techniques: powder metallurgy (sintered magnets) or rapid solidification (bonded magnets). Usually energy products (BH)max are obtained in the range of 20-40 MGOe [15].

On the other hand, these permanent magnets usually have a lower Curie temperature of approximately 300-325°C. As such they cannot be used for very high temperature applications. Also Neodymium is usually reactive and hence there is a tendency of these magnets to corrode easily.

1.6.2 Objective – From the phase diagram it is understood that the cooling rate affects the microstructure and therefore we can tailor the microstructure by controlling the wheel speeds. It is seen see that a wheel speed of 10m/s will result in a slower cooling rate and therefore there is a greater tendency to form α-Fe phase, for the $Nd_{10}Fe_{84}B_6$ sample from the liquid phase. However, if it is cooled cool at 20m/s, then from to the phase diagram, it is seen that it is easier to come down quickly to the 2-14-1 phase and the amount of α-Fe formed is less. Therefore by controlling the cooling rate and thereby indirectly controlling the phases present (the percentage of the hard and the soft phase) it is possible to control the phase formation.

1.7 MnIr-Fe SYSTEM: The phase diagram of the Mn-Ir system is shown in Figure 1.11.

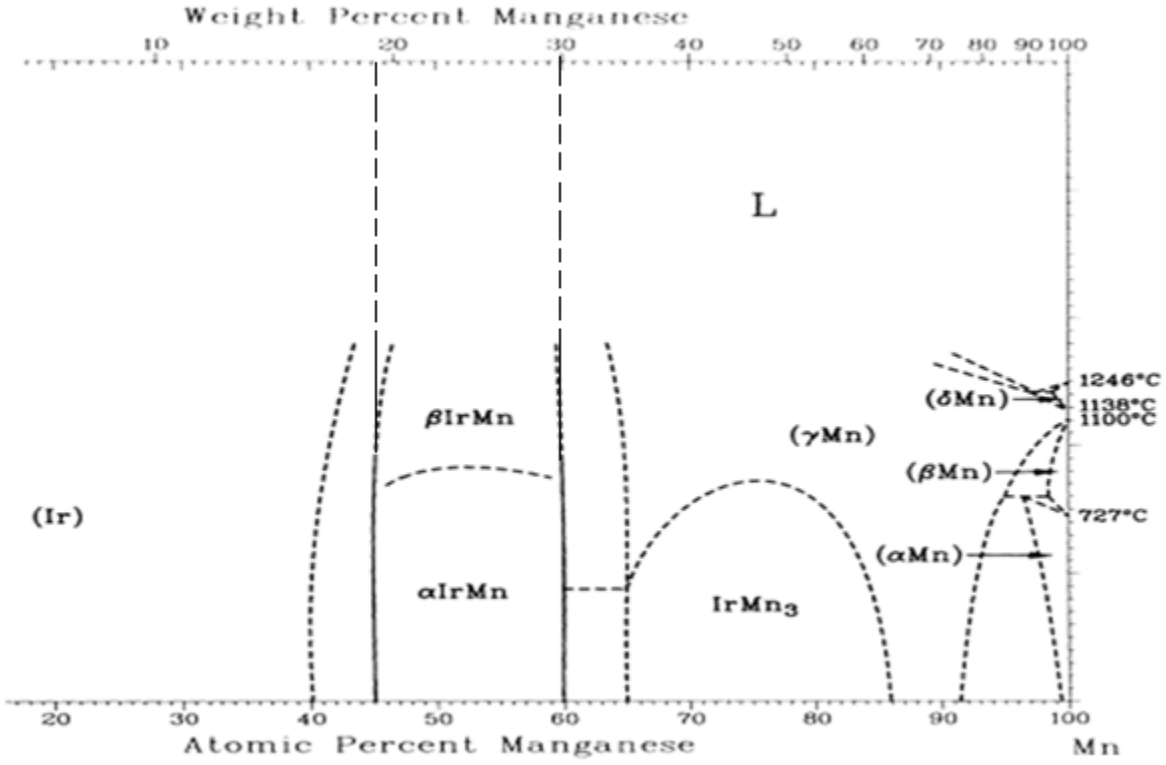

Figure 1.11: *Phase Diagram of the Mn-Ir system* [8].

1.7.1 Objective – It has been observed from previous experimental data that the $L1_0$ MnIr phase is antiferromagnetic. This indicates that the alignment or orientation of the spins in the phase are antiparallel to each other i.e. there is one layer of spins aligned in a particular direction, and the next layer of spins are aligned in exactly the opposite direction i.e. they are 180 degrees with respect to their adjacent layers. It has been suggested that such antiferromagnetic materials have a high degree of exchange anisotropy and therefore they can be put to various applications.

It has also been noted experimentally by various observers that the MnIr equiatomic alloy exhibits the $L1_0$ crystal structure. Therefore the objective is to form antiferromagnetic equiatomic MnIr alloy and then exchange couple it with a softer ferromagnetic metal such

as Fe. The high antiferromagnetic stability (high Nẽel Temperatures) and exchange anisotropy coupled with the soft ferromagnetic properties of Fe, and then nanocomposites can be obtained which has the better qualities of both its components and give us a permanent magnet with high coercivity as well high magnetization. Alloying of Mn and Ir were done carefully by arc melting, as Mn tends to splatter all over the arc melting chamber as it has a high vapor pressure. Formation of the nanocomposite was initiated by mechanical milling of the MnIr alloy with Fe, so that intimate contact of the grains took place.

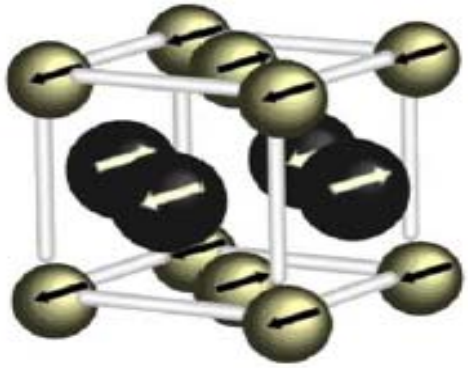

Figure 1.12: *This represents the hypothetical representation of an L1₀ structure (MnIr in our case) having antiferromagnetic spin alignment* [5].

2. EXPERIMENTAL TECHNIQUES AND EQUIPMENT

2.1 SAMPLE SELECTION AND PREPARATION:

This essentially involves measuring out the standard weights of the samples carefully, in the ratios that we need to make the necessary alloys.

2.2 ARC MELTING:

Arc melting is a technique used to melt metals under an electric arc that is struck by a high applied voltage. The arc melts the metals and then when they solidify, the required alloy is usually formed. It should be noted that arc melting is usually done in an inert atmosphere so as to prevent the formation of any oxides as very high temperatures can be reached**.** The arc is usually struck with the help of an electrode tip.

Arc melting is done to obtain the alloy from the respective elements. The samples are kept in the melting chamber and then the chamber is closed and purged a number of times with Argon gas. This is done so as to remove any traces of oxygen that might be present. This oxygen will oxidize the sample at the high arcing temperatures reached and therefore it must be removed. Usually the purging is done 5-6 times. The base pressure that was reached for this was 60 millitorr.

A Zirconium piece is kept at a certain distance away from the sample and once the arc is struck, it is brought in close proximity to the Zr piece and it is allowed to be melted. After the piece has solidified back, we check to see if there is any tarnishing on the piece which would then be indicative of any oxidation. If the Zr piece remains untarnished then we can go ahead with the arc melting of the individual elements to form the alloy. Once the individual elements are melted to form the ingot it is then flipped over and re-melted again

to obtain a uniform melt. Once this is done, the required alloy is retrieved after it has been allowed to cool down for a few minutes.

2.3 MELT SPINNING AND RIBBONS:

Melt Spinning is a very important non-equilibrium process. This process is used to cool molten metals very rapidly. This process is used to make ribbons in my case. Some of the steps involved in the melt spinning can be outlined as:

i) Obtaining the hole at the bottom of the crucible and then loading the crucible with the sample in it inside the melt spinning chamber.

ii) Purging the chamber repeatedly (3 times) to remove any traces of Oxygen which might oxidize the sample due to the high temperatures attained.

iii) Rotating the wheel at the required speed.

iv) Shooting the molten sample towards the spinning wheel to form the ribbons.

v) Collecting the ribbons.

The melt spinner is from Edmund Buehler Company. We initially take a crucible and then get a hole of about 0.5mm. The crucible is loaded with the sample and tightened inside the chamber. Then the chamber is repeatedly put under vacuum and flushed with Argon. The final pressure that we go down to in this case is approximately 2.3E-2. The wheel was set to the desired speed and then the chamber was heated with a RF induction coil. Once the desired temperature is reached and the sample has melted we open the valve and shoot the sample such that the ribbons are obtained. The ribbons are now ready for XRD analysis and further measurements.

2.4 MECHANICAL MILLING:

The word “milling” usually refers to the breaking down of coarser particles to finer sizes. Milling is applied in ores, in industries e.g. to break down quartz to fine powder etc. [20].

Therefore it is understood that the main objective of the mechanical milling process is the reduction in particle size, mixing and blending etc. The most important fact to note here is that mechanical milling involves the repeated welding, fracture, rewelding of the powders involved. It can be basically summarized as a process where the forces generated caused by the vibratory motion of the vials act on the milling charge i.e. the balls and the powders. The milling media and the powders alternatively roll on the inner wall of the vial and are lifted and thrown off across the bowl at high speeds.

Now nanocomposites have recently attracted a lot of attention as they provide enhanced nanoscale properties and smaller reinforcing particles [20]. Also mechanical milling provides the following advantages:

a) Since it is done mostly at room temperatures, we can overcome the disadvantages of the liquid metallurgy process.

b) very homogenous and uniform nanocomposites are produced in this case.

For my experimental purpose, the SPEX 800 automated ball milling machine is used. The ball milling vials are made of hardened steel and a record of the ratio of powder to the weight of the balls is kept. The vials are sealed with the powder and milling balls inside in a glove box in an inert atmosphere (Nitrogen or Argon). Then they are fixed in the milling machine allowed to run for the required amount of time. Usually the machine's run time cycle is controlled by a microcontroller and it is allowed to run for ten minutes and then stop for ten minutes. This process is usually done so that the powders do not get oxidized due to the very high temperatures that can be reached locally. Once the milling of the required time is done, we take the sample out and check whether the required phase has formed, by using x-ray diffraction.

2.5 ANNEALING:

Annealing is a very important technique in metallurgy. It is a heat treatment technique whereby we use elevated temperature to facilitate the formation of a phase; as such high temperatures provide energy needed for the diffusion of the atoms. The heat energy increases the diffusion rate and there is movement of the atoms. This therefore leads to the reduction of dislocations and as a result, the reduction of stress. Also it is noticed that a change in the mechanical properties of the material, e.g. in hardness and ductility. Annealing, therefore, has a very significant role to play in metallurgical processes. Also, a phase transformation takes place and therefore annealing can be a technique to obtain a phase that is desired by us. After the heat treatment however, the cooling rates can be varied: it might either be slow cooling or very rapid cooling or quenching.

For experimental purposes, the sample is placed in a quartz tube and the Oxygen is purged several times. This process is necessary as the present of even very small quantities of Oxygen can react with the sample forming Oxides, especially at high annealing temperatures and thereby rendering the process ineffective. Now, once the sealing is done, the sample inside the evacuated quartz tube is placed inside the tube furnace. Usually, the furnace is switched on sometime so that it reaches the proper temperature before the sample is inserted. After the heating is done for the required amount of time, we switch the furnace off and allow some time for the quartz tube with the sample to cool down (provided we are not doing any quenching). Once it comes back to the room temperature, it is ready to be characterized.

2.6 X-RAY DIFFRACTION:

X-Ray Diffraction technique is one of the most important techniques for characterizing a material, especially if it is crystalline. X-Rays are electromagnetic radiation of high frequency (consequently low wavelength) that can be used to study the structure of crystalline materials since their wavelengths of these X-Rays are almost comparable to the lattice parameters of the crystalline materials. Therefore X-rays are regarded as one of the most important tools in studying the structure of matter. X-Rays are usually generated by two methods:

a) when high speed electrons striking a target slow down, they liberate energy continuously resulting in a continuous X-ray radiation (also called "Bremsstrahlung" or Braking Radiation").

b) when the impinging high speed electron has sufficient kinetic energy to knock out an electron from the inner shells (K, L or M shells) of the target atom, then the atom gets excited. To get it back to a stable state, an electron from a higher energy shell drops down to fill this hole and the resulting energy is liberated in the form a characteristic X-ray i.e. characteristic to the energy difference to the two shells in for that atom. This type of X-ray is usually non-continuous.

It is well understood that crystalline materials exhibit an ordered arrangement of atoms which are spread over a long range i.e. a long a range atomic order. The typical interatomic spacing is approximately 2-3Å and since the wavelength of the X-rays are of that order, they are extensively used to study the structure of crystals by diffraction techniques. The interaction of X-Rays with crystals can be understood by the fact that the X-rays directed towards the crystal interact mainly with the electrons of the atoms in the crystal. The scattering of X-rays from the atoms takes place mainly through the electrons of the atoms in the crystal. Secondary waves are generated when these X-rays collide or scatter with the

electrons. This scattering takes place in all directions. And also as there approximately a million atoms in a “piece” of a crystal, these scattering takes place in all possible directions. However, these scattered secondary waves are strongest only in those directions in which they are in phase and the scattering is additive or we say there is constructive interference. In most other cases the directions of scattered secondary waves are such that they cancel each other out and no considerable intensity is obtained. This is called destructive interference. The constructively scattered beams are detected by an X-Ray detector.

The principle of this constructive diffraction technique is understood with the help of Bragg’s law which can be mathematically written as:

$$n\lambda = 2d \sin\theta$$

Bragg’s law considers the crystal as a set of parallel planes and a beam of X-Rays of wavelength λ being incident on them. In this consideration, the interaction between the X-ray beam and the electrons of the atoms is similar to a kind of reflection, similar to the diffraction by a three dimensional grating. The incident angle of the X-Ray beam on this atomic plane i.e. the Bragg angle θ is equal to the reflected angle. When the path difference between the rays reflected from two adjacent atomic planes are an integral multiple of each other, there will be constructive interference, and otherwise there is destructive interference. Bragg’s law can be schematically represented as shown below:

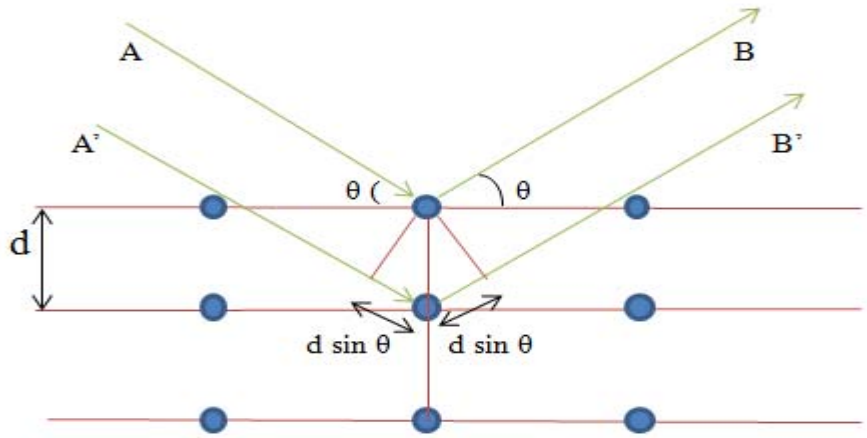

Figure 2.1: *This represents the Bragg's law schematically.*

2.6.1 Powder X-Ray Diffraction:

Powder X-ray Diffraction is a technique that is usually used as an application of Bragg's law to obtain the phases present and consequently the structure of the crystal lattice. The size and shape of the unit cell can also be obtained by this technique. A RIGAKU Multiflex X-Ray Diffractometer is used in this case. The powder is usually obtained by crushing the ribbons thoroughly in a mortar and pestle. A powder sample essentially means a polycrystalline sample. This powder is placed on a zero background slide and the slide is placed in a holder which is fixed with a pair of screws. Once the X-Ray is switched on the Diffractometer adjusts the θ-2θ position based on the angle settings we have put in. The crystals arranged randomly in the sample diffract the X-ray beams based on their relative orientations and the net diffraction intensity is noted by the detector. The X-ray pattern (graphical representation of intensity peaks) is particular for any particular material (or

phase) and we can correctly identify the phase present by studying the X-Ray peaks obtained.

The peaks obtained contain a lot of information about the structure of the crystal as well as the shape and size of the unit cell. The various peak parameters are the peak width, the peak positions and the peak intensities. The peak width is the resultant of grain size and strain in the crystal as well as any instrumental error, whereas the peak positions indicate the size and shape of the unit cell. The peak intensities tell us the position of the atoms. When the incident beam strikes the powder sample, the diffraction takes place in every possible 2 theta orientation. The diffracted beam is detected by the moveable detector. And the data is matched with standard data from the JCPDS files.

2.7 RIETVELD ANALYSIS:

Rietveld Refinement is a powerful technique that is used to characterize and study the structure of crystalline materials. It is usually used to refine the parameters that are obtained as output from the X-Ray diffraction data. Some of the parameters that are refined include lattice parameters, peak width and shape and preferred orientations [19]. Non-Rietveld analysis uses an integrated analysis to understand the peak parameters, whereas in the Rietveld analysis we use the complete peak profile instead. The formula used here is:

$$(Y\ i)\ \text{calculated} = \Sigma\ (F\ ^{(hkl)^2}\ (hkl)\ (TF)\ (LPF)\ (\text{Line Shape/H}))$$

Where Yi is the intensity of each point in the profile, LINE SHAPE is a Gaussian function and H is the half width of the phase line. The main advantage of the Rietveld analysis is the fact that results are far more accurate and since it follows an iteration process, the errors are much lesser. FULLPROF software was used for performing

RIETVELD analysis. The minimum chi square values are usually taken and are considered to be the best fit.

2.8 ALTERNATING FIELD GRADIENT MAGNETOMETER (AGFM):

The AGFM is used for the magnetic measurements i.e. the measurements of the hysteresis loops of the various samples are done with the Alternating Field Gradient Magnetometer or Vibrating Reed Magnetometer commonly called the AGFM. The AGFM is a device that was first devised by Ziljstra when he arranged to position a tiny sample within a dc field having a relatively lesser alternating gradient. The instrument is capable of applying a given quantity of magnetic field on the sample. Also there must be a source of an alternating field which is applied. As a result, the sample oscillates which can be detected and determined with the help of a sensor which takes the corresponding displacement into account. Basically a homogenous alternating field gradient is produced at a closely controlled frequency with the help of the AC coils. Iron pole pieces are used and their function is to provide a proper frequency relation and dependence between the amplitude and phase of the given field. The resonant nature of this type of magnetometry is the central functioning parameter of the AGFM setup. Usually we want a higher value of sensitivity and a considerable amount of mechanical gain. The sensitivity of the AGFM is denoted by the Q factor where Q = Sr/Ss where Sr is the sensitivity at resonance and Ss is the static sensitivity. Therefore to detect the magnetic properties of small samples, the values of these sensitivities have to be considerably large. Another thing that is important to note here is that the resonance peak's width is determined by the Q factor, and as such a lesser Q value indicates a broader peak. Now, when we mount the sample, it is understood that the sample is under the effect of the external magnetic fields as well as the moments acting upon it due to its own field. This self-moment needs to be small so that contributions due to background can be neglected.

The sensitivity of the AGFM is usually much more than a Vibrating Sample magnetometer (VSM), approximately about 80-100 times. However, the maximum sample and the geometry of the sample that can be used is limited for a AGFM as against a VSM. The entire AGFM set-up needs to be tuned to its resonant frequency for each different sample mass, however, the powerful software system usually takes care of this. Changing the field gradient can be an issue sometimes; however this problem is usually encountered when measurements are being done for soft magnetic materials.

3. EXPERIMENTAL PROCEDURES

3.1 Nd-Fe-B SYSTEM: Two different Nd-Fe-B were used i.e. $Nd_{12}Fe_{82}B_6$ and $Nd_{10}Fe_{84}B_6$. Also the preparation of these samples has been done at two different wheel speeds of 10m/s and 20m/s. Therefore there are have basically four different samples considering the compositions and wheel speeds. Carefully weighed quantities of each sample were taken before the arc melting process. This can be enumerated as follows:

Composition **Wheel Speed**	**$Nd_{12}Fe_{82}B_6$**	**$Nd_{10}Fe_{84}B_6$**
10m/s	5.5g	5.85g
20m/s	6.2g	5.45g

The arc melting is done carefully in an Argon atmosphere. The samples were kept in the chamber and it is purged about five times to make sure that any traces of Oxygen are removed. The arc melting takes place at very high temperatures and any trace Oxygen present will oxidize the sample and therefore render it useless for further use. The pressure is taken down to approximately as low as between 60 and 100 millitorr progressively with each purging. The arc melting is done at a pressure of approximately 80 millitorr which is the optimum. Once the melting has been done, then the ingot is allowed to cool for some length of time (approximately 5 minutes) before it was flipped over with the tip of the electrode and melted once again. This is done to ensure homogeneity. Once this is done, the sample was allowed to cool again and then taken and weighed back in the balance. This

is done to check that there has been not much of a weight loss. Again, the weights of the samples obtained and the starting weights can be tabulated as follows:

Composition	**Wheel Speed**	**Initial Weight of individual elements**	**Final weight of ingot**
$Nd_{12}Fe_{82}B_6$	10m/s	5.50g	5.44g
$Nd_{12}Fe_{82}B_6$	20m/s	6.20g	6.00g
$Nd_{10}Fe_{84}B_6$	10m/s	5.85g	5.50g
$Nd_{10}Fe_{84}B_6$	20m/s	5.45g	5.40g

After arc melting, the samples are melt spun using a single-roller melt spinner. As mentioned above, melt spinning is a rapid solidification technique used to produce very high cooling rates so that nanocrystalline grains are obtained. Once the sample is ready (it has melted) the melt spinning wheel is turned on at the required speed (10 and 20m/s in our case for both the samples) and then the valve is opened. This applies the pressure, the sample is shot downwards and once the liquid metal falls on the spinning wheel, ribbons are formed. After allowing the chamber to cool for some amount of time (approximately 5-10 minutes), the wheel is slowly turned off and the ribbons are collected. The ribbons are carefully collected and kept in a container and the crucible is discarded.

Once the ribbons have been obtained, they are crushed thoroughly so that powder XRD can be done. The sample powder sample is now mechanically milled at different time periods of 15minutes, 30minutes, 60minutes, 90minutes and 120minutes. For the mechanical milling care is taken to see that the sample vials are closed under an inert atmosphere. This is done so as to prevent oxidation of the sample, as localized high

temperatures can be reached during the milling process. Now, at each step of the milling process, after the given time, some amount of sample is taken for powder XRD to monitor microstructural evolution and magnetic behavior as a function of milling time.

3.2 MnIr-Fe SYSTEM: The first process in obtaining this alloy system is the formation of the MnIr system. Therefore, first the samples were weighed out carefully to obtain the required amounts necessary. Initially, both the Mn and the Ir samples were weighed out and care was taken to see that they were equiatomic. From the phase diagram of the Mn-Ir system and also from theoretical molar calculations it is found out that equiatomic Mn:Ir ratio corresponds to weight percentages of 77.72% Ir and 22.28% Mn, respectively. The weighing was done very carefully (about three times) for each element to make sure that there were no mistakes because errors in the weighing might result in the phase not being formed. The respective weights of the samples taken were 3.7 g of Iridium and consequently 1.0607 g of Mn respectively.

Initially MnIr equiatomic alloy was tried to be formed by the method of mechanical milling. The milling was done for progressive time intervals in sealed hardened steel vials as described above. However after approximately 150 minutes of ball milling it was noticed that there were some peaks of IrMn (as checked from the JCPDS files), however there were still peaks of elemental Ir and elemental Mn which seemed to indicate that the alloy formation was not taking place. To overcome this problem another approach was tried.. Again, equiatomic amounts of sample were carefully weighed out which corresponded to 3.5 g of Ir and 1.0034 g of Mn respectively. However this time instead of mechanical milling technique, the samples were arc melted.

The arc melting procedure was carefully done. The samples were placed in the thoroughly cleaned chamber, and then the pressure inside the chamber was pumped down about 6

times with the base pressure reaching approximately 60 millitorr. Each time the chamber was purged with Argon gas. This process, as explained above is done to remove any unwanted Oxygen that might have been present which could have oxidized the samples at the high temperatures reached, especially Mn which is more reactive. After the purging is done, the arc is struck with the help of the electrodes and the Mn and Ir elements are melted. The melted ingot was flipped over with the tip of the electrode after it has cooled and remelted so that the melt obtained is uniform.

The arc melter was allowed to cool for some time (there is a water circulating system) which helps in this process and then the sample is taken out and weighed to check the weight loss. It was found that that the net weight after melting 4.4801 g which indicates a weight loss of 0.0233 g or 0.517% which is acceptable as that still makes the sample to stay within the phase boundaries as indicated from the phase diagram. After arc-melting, one surface of the ingot was polished so as to obtain a flat and smooth surface. Once a smooth polished surface was obtained, an X-ray diffraction was done with the solid arc melted ingot. However, from the as cast sample, the diffraction peaks that were obtained were only the (111), (200) and (202) peaks indicating that even though the ingot has been formed in the equiatomic ratio, the phase formation has not completely taken place.

The arc melted ingot was now taken for annealing. Annealing is a very important phenomenon in most of the metallurgical techniques. It helps in the phase formation as it provides the energy necessary for the atoms to diffuse. Annealing helps in reducing or relieving the internal stresses and also improves the ductility of the material. Annealing can be considered to be helping the alloy reach its equilibrium state. We seal the ingot is carefully sealed in silica tube and then anneal the sample in a box furnace at 700 C for 3 days. After 3 days the sample is allowed to cool down slowly (rapid quenching is not done) and then once again an X-Ray diffraction analysis of the sample is done. This time it is

found that almost all of the peaks correspond to those of MnIr. X-Ray files as well as Rietveld analysis technique is used for this matching.

After this Fe powder was added to MnIr in 1:1 weight ratio to study the effect of exchange interaction. The Fe is a soft ferromagnetic material and it is expected to exchange couple with the antiferromagnetic MnIr phase. For this, the samples are mechanically milled at progressively increasing time intervals. Again as noted before, the mechanical milling is done in a hardened steel vial which is sealed in an Argon atmosphere. This was done to prevent the oxidation of the sample at the high temperatures that are reached locally due to the mechanical milling process. This is done so that it results in the two components coming together intimately and alloying together, this will help in effective exchange interaction at the interface. After ball milling for successive time intervals, take out small amounts of the sample at each stage are taken out and an X-ray analysis and a magnetic measurement (AGFM) are done at each stage. Similarly small amounts of the sample is taken at each stage and anneal them at 700C for 15 minutes and note their magnetic properties in the AGFM. As a representative, the X-ray patterns of the samples of 14 and 16 hour mechanical milling are also noted.

4. RESULTS AND DISCUSSION

4.1. Nd-Fe-B SYSTEM – The first step was the weighing of the different elements in the balance. Followed by that, careful arc melting was done and then the ingot formed was checked for any loss of mass and I proceeded if the mass loss was not considerable enough. After that melt spinning was done to obtain the ribbons at the necessary wheel speeds. Once the ribbons were obtained, they were crushed thoroughly to be prepared for powder XRD analysis and magnetic measurements. Mechanical milling was done carefully on the samples (in Nitrogen atmosphere) for progressively increasing time intervals of 15mins, 30mins, 60mins, 90mins, and 120mins. Also after each stage of ball milling some amount of sample was taken out of the milling vial for powder XRD and also weighed for magnetic measurements in the AGFM.

4.1.1 Powder XRD Results: X-ray diffraction (XRD) was used to characterize the as-solidified alloys after melt spinning (Figure 4.1). The predominant phase in all four samples was Nd2Fe14B. Only the strongest lines are indexed in Figure 4.1 due to the complexity of the diffraction pattern; all peaks (except those belonging to a-Fe) can be indexed to the Nd2Fe14B phase. Also present in the XRD patterns were peaks corresponding to a-Fe. As expected, the alloys with a lower Nd content appear to have a higher phase fraction of a-Fe, based on diffraction peak intensities.

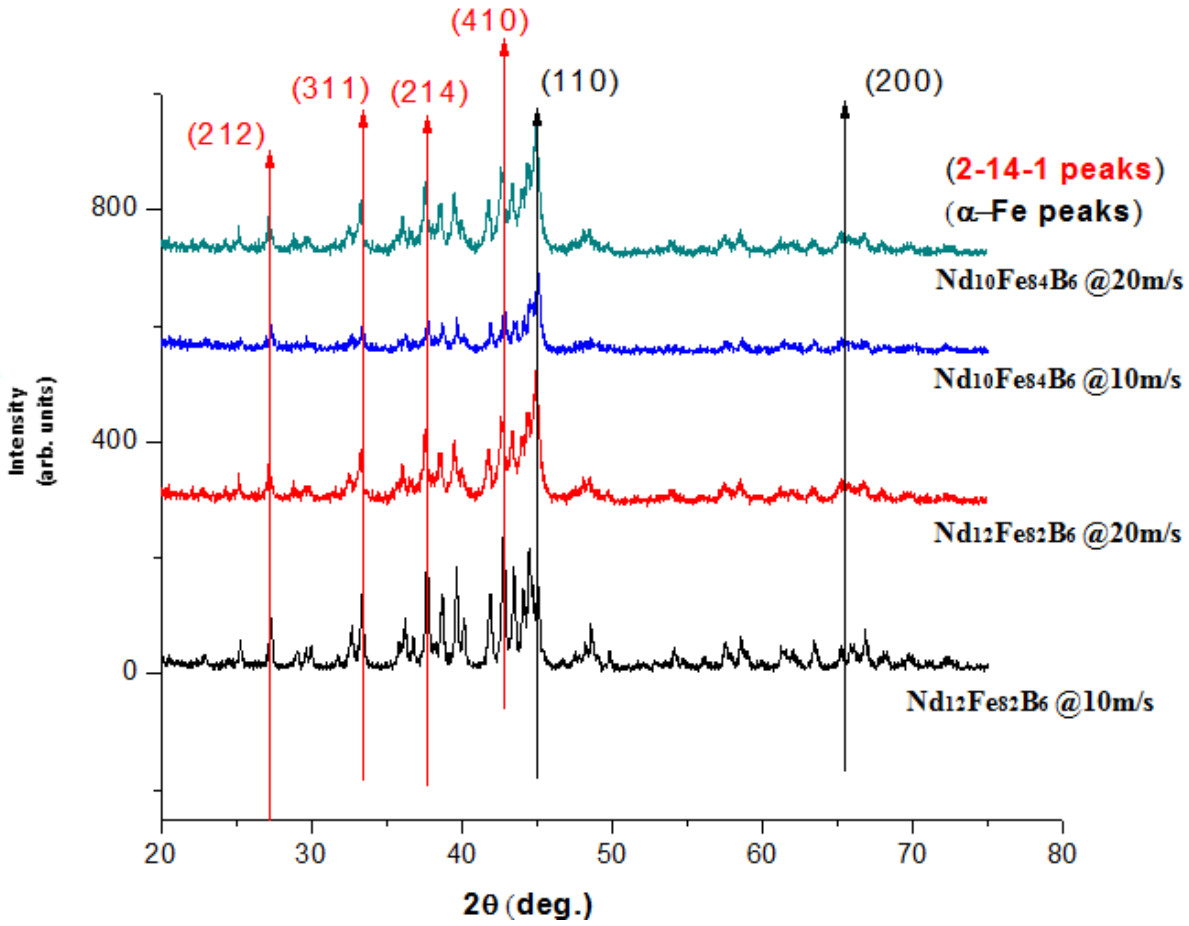

Figure 4.1 *This represents the as spun (not milled) XRD peaks of the four different samples at their respective wheel speeds.*

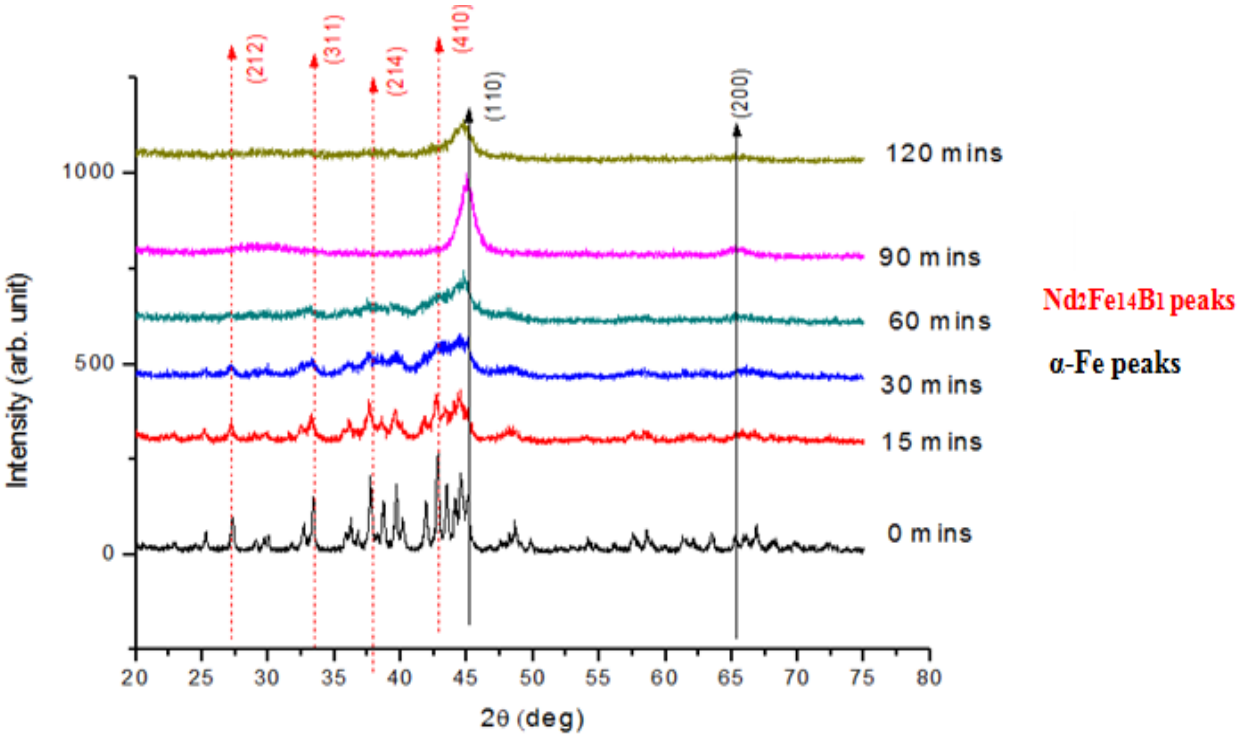

Figure 4.2 *Graphs showing the powder XRD patterns of* $Nd_{12}Fe_{82}B_6$ *melt spun at 10m/s, with increasing milling times.*

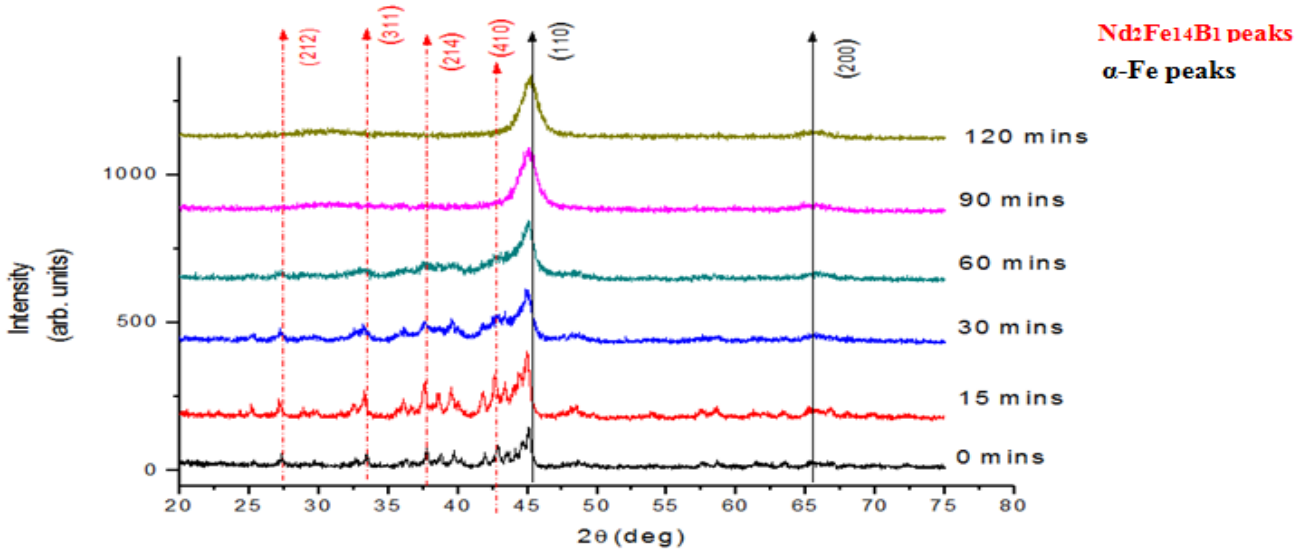

Figure 4.3 *Graphs showing powder XRD pattern of* $Nd_{10}Fe_{84}B_6$*, melt spun at 10m/s with increasing milling times.*

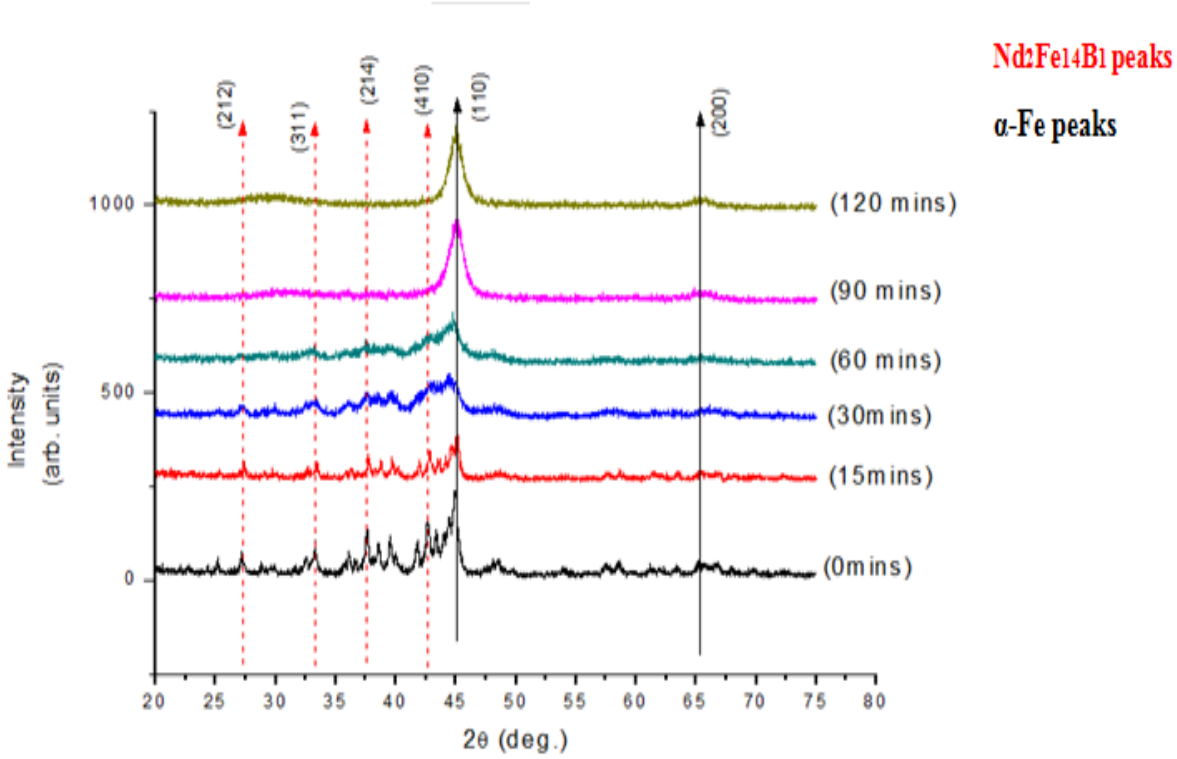

Figure 4.4 *Graphs showing powder XRD pattern of* $Nd_{12}Fe_{82}B_6$*, melt spun at 20m/s, with increasing milling times.*

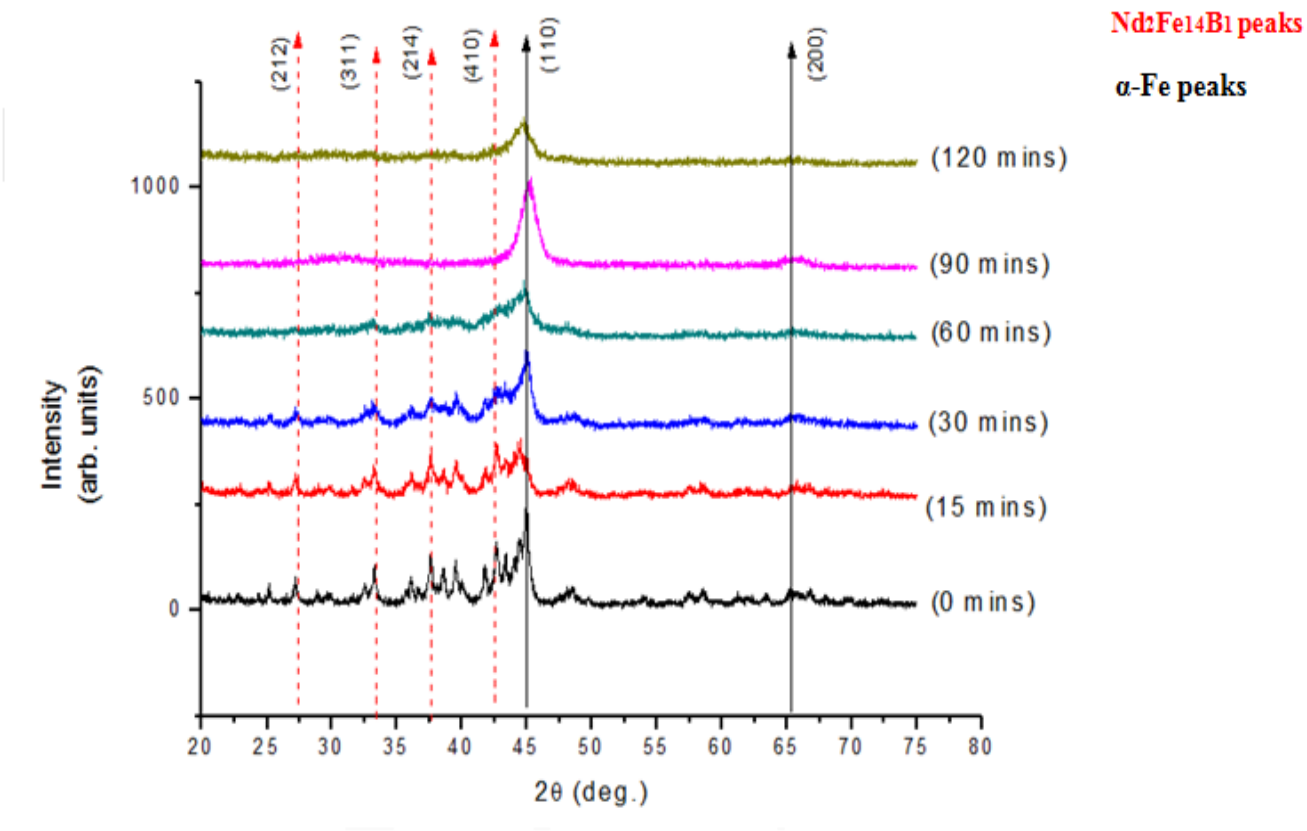

Figure 4.5 *Graph stack showing powder XRD pattern of $Nd_{10}Fe_{84}B_6$, melt spun at 20m/s, with increasing milling times.*

Each of the melt spun samples was mechanically milled for times up to 120 minutes. Structural changes were monitored by XRD, while changes in magnetic behavior resulting from the milling were measured by AGFM. In general, mechanical milling resulted in an initial decrease in grain size, as indicated by the overall broadening of the diffraction peaks. After 60 minutes, significant structural disorder was introduced, as the diffraction peaks evolved into generally broad, diffuse peaks. At 90 minutes, no peaks corresponding to the Nd2Fe14B phases remain. From the **Figures 4.1, 4.2, 4.3, 4.4** and **4.5** some trends are observed. The figures each represent the XRD patterns of the $Nd_{12}Fe_{82}B_6$ and $Nd_{10}Fe_{84}B_6$ samples at 10m/s and 20m/s wheel speed respectively. The most important feature that we observe here is that in all the 4 samples consist of a 2 phase system in the as spun condition, i.e. when they have not been subjected to any mechanical milling at all. This is especially seen from Figure 4.1, which shows the as spun XRD data

of both the samples at 10m/s and 20m/s. Also here, the 2 phases are $Nd_2Fe_{14}B$ (2-14-1) and α-Fe phase. The main peaks of the 2-14-1 phase and the α-Fe peaks have been labeled in red and black respectively.

From the subsequent **Figures** (**4.2 to 4.5**) we notice some important observations. Firstly we notice that there is a gradual decrease in relative intensity of the XRD peaks with progressively increasing milling times. There is also a relative increase in the peak widths with respect to the base graph i.e. graph representing the as spun condition (0 minute mechanically milled) in every case. This can be attributed to the fact that the particle sizes go on reducing with more and more mechanical milling and ultimately it tends towards becoming amorphous. Also strain is introduced due to the continuous bombardment of the hardened steel balls on the crystallites. In the final milling period i.e. 120 minutes, we notice that it has finally become one single phase and the rest is mostly amorphous.

Another important observation, especially from **Figure 4.1** is that the average relative intensity of the peaks is more for the $Nd_{12}Fe_{84}B_6$ sample for both the wheel speeds vis-à-vis the $Nd_{10}Fe_{84}B_6$. This can be understood from the fact that the 2-14-1 and the α-Fe phases are formed better due to the lesser wheel speed, whereas the faster wheel speed and consequently greater cooling rate results in incomplete formation of the crystallites.

4.1.2 Magnetic Measurements: Magnetic measurements were done with the samples for both melt spun at 10m/s and 20m/s. The AGFM was used for performing the magnetic measurements. Magnetic measurements were made for all the mechanically milled samples at the different time intervals. It is important to note that the AGFM measurements give the hysteresis and the value of the coercivity. However, the magnetization values thus obtained are not normalized and therefore have to be divided with the sample mass to obtain the proper magnetization in emu/g. I have used the parallel probe for performing the magnetic measurements. The optimum hysteresis loops for the compositions at the two different wheel speeds are given as under:

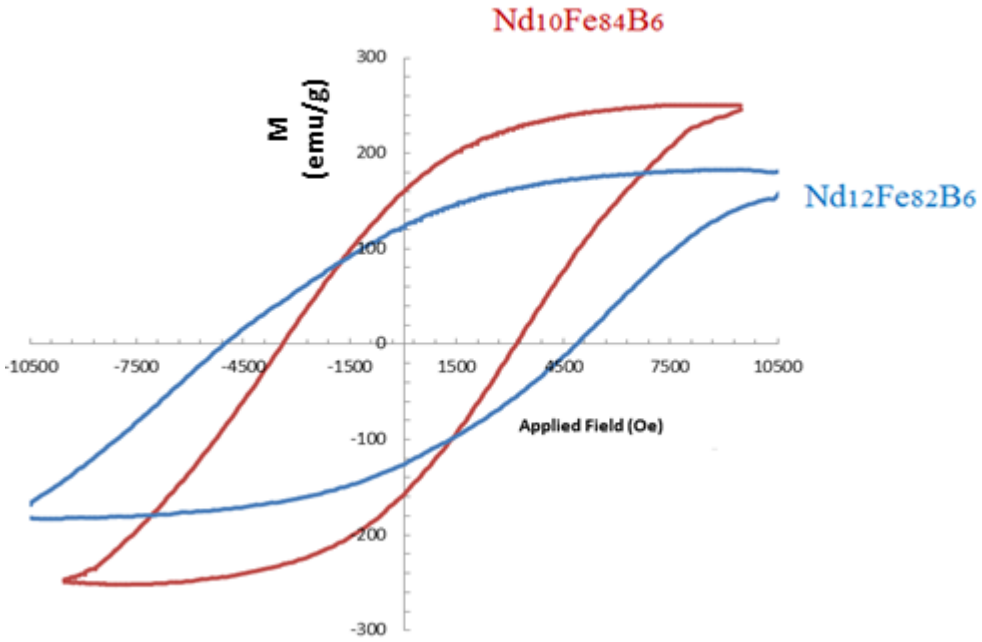

Figure 4.6 *Graphs showing the optimum hysteresis loops of the samples melt spun at 10m/s.*

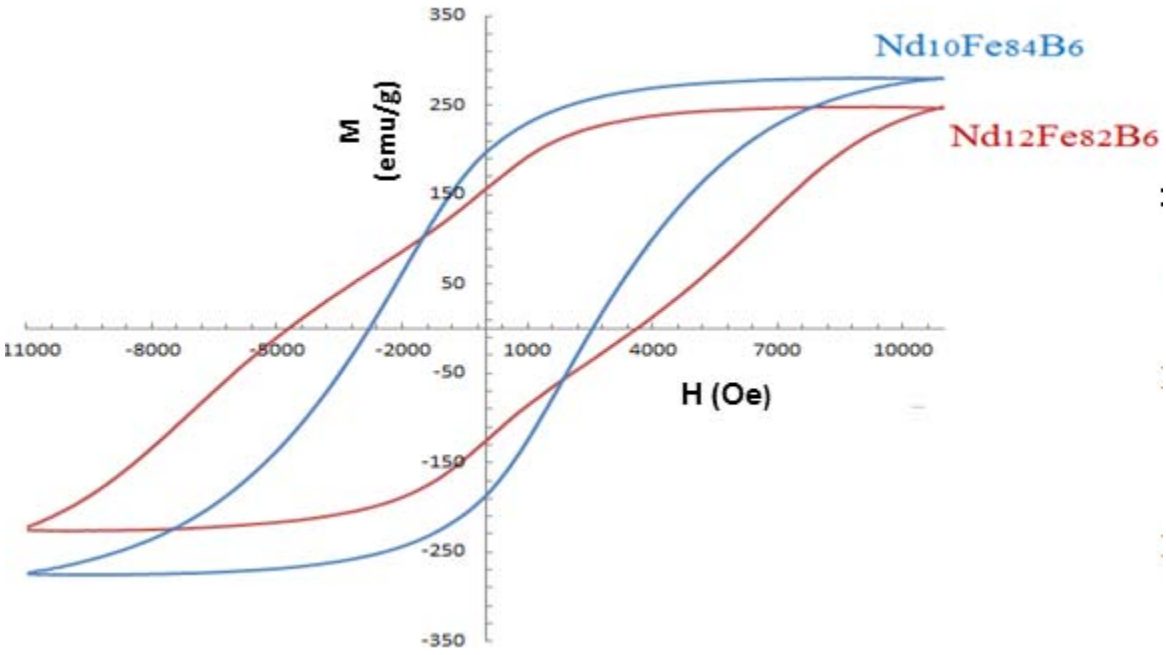

Figure 4.7 *Graphs showing the optimum hysteresis loops of the samples melt spun at 20m/s.*

The **Figures 4.6** and **4.7** show the optimum hysteresis loops of both the compositions at the two different wheel speeds, i.e. 10m/s and 20m/s respectively. It is observed in both that the cases that the $Nd_{12}Fe_{82}B_6$ sample has higher value of coercivity at than the corresponding $Nd_{10}Fe_{84}B_6$

sample. This observation can be attributed to the fact that the $Nd_{12}Fe_{82}B_6$ sample has a lesser quantity of α-Fe (the soft magnetic phase).

4.1.3 Effect of Mechanical Milling: We now consider how the effect of the mechanical milling by comparing the two samples. The comparison is done mainly as a comparison of the hysteresis loops of the samples for the different milling times and also as a graphical analysis of coercivity versus the milling time for both the samples at the two different wheel speeds. The graphical representations are tabulated as under:

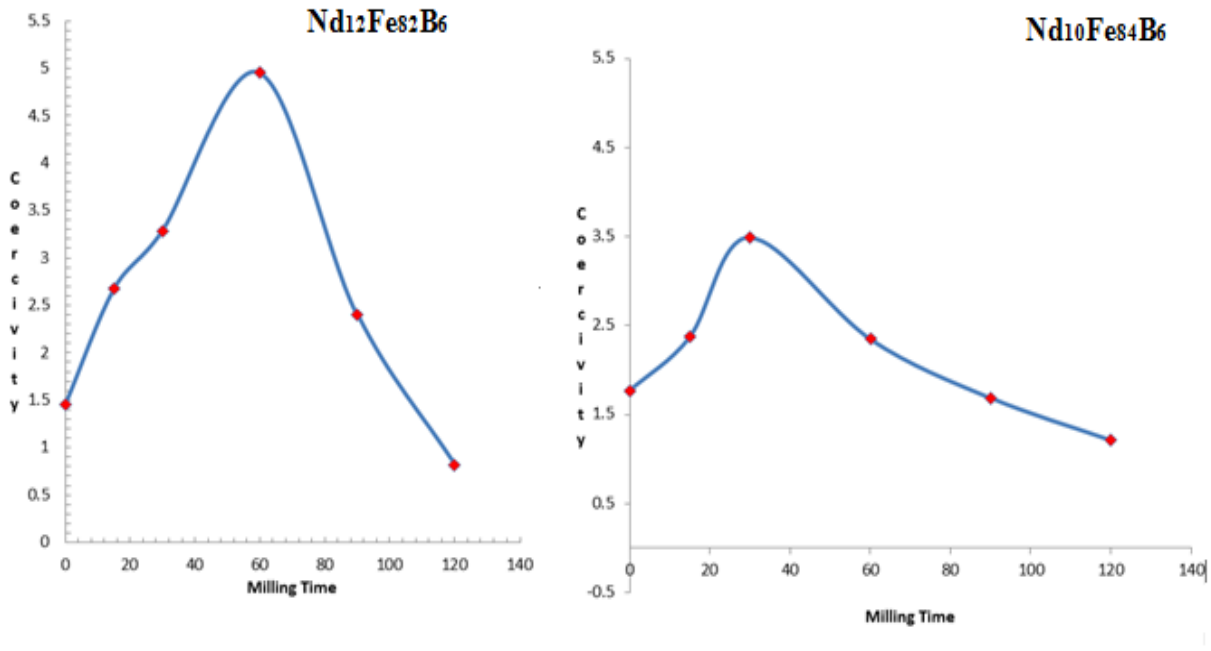

Figure 4.8 *Comparison of coercivities of the two samples at a wheel speed of 10m/s.*

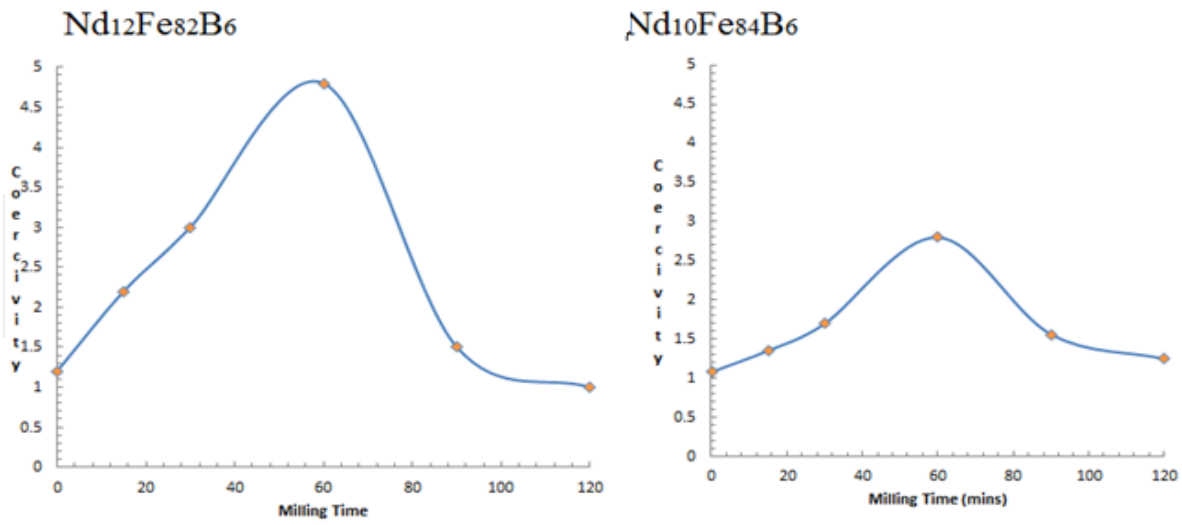

Figure 4.9 *Comparison of coercivities of the two samples at a wheel speed of 20m/s*

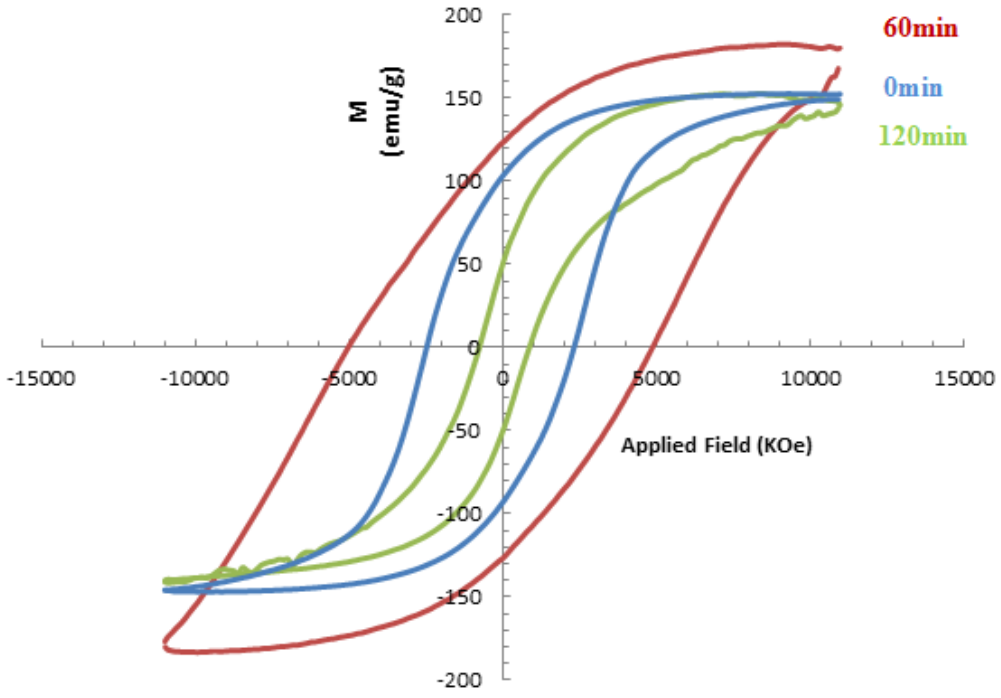

Figure 4.10 *This shows a comparison of the coercivities of the $Nd_{12}Fe_{82}B_6$ samples melt spun at 10m/s at different milling time intervals as a comparison.*

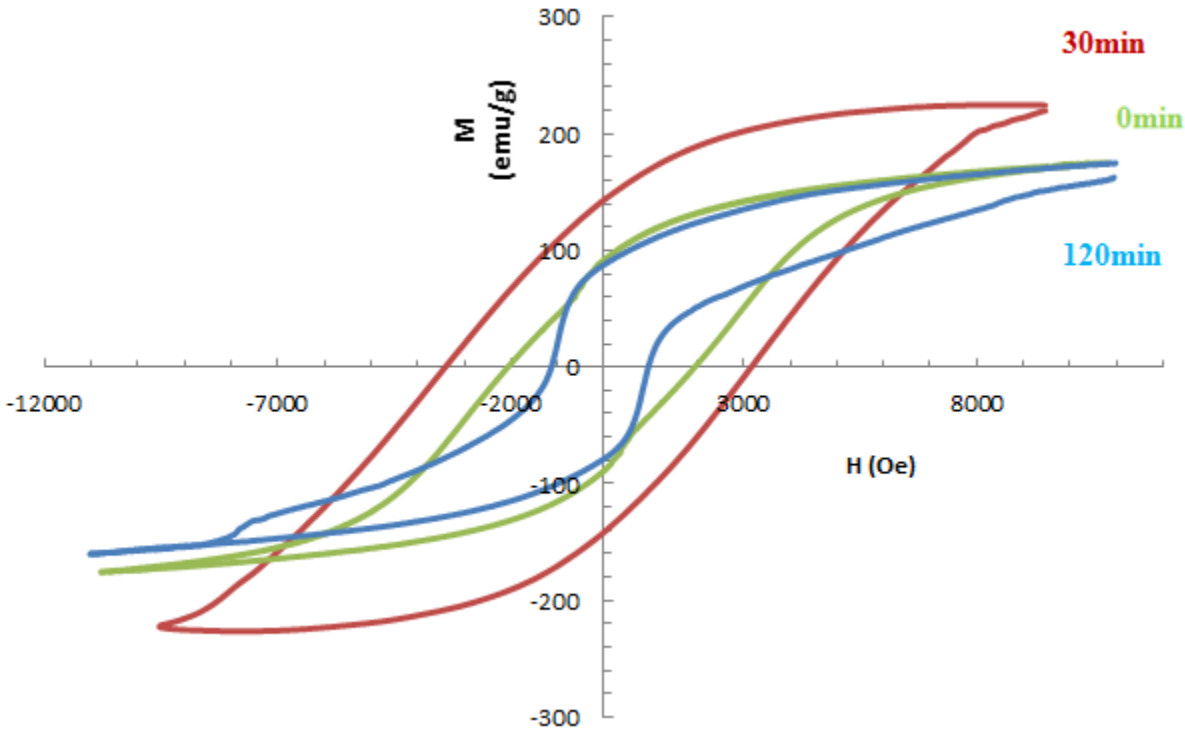

Figure 4.11 *Optimum coercivities of the $Nd_{10}Fe_{84}B_6$ samples, melt spun at 10m/s, as a function of milling time.*

From the Figures 4.8 4.11, we notice some important observations. Firstly it is seen that the coercivities of both the samples tend to increase with the increasing ball milling time intervals. This is because the particle sizes go on decreasing and thereby the coercivity increases. However, it is seen also from the graphs that the coercivity falls off with further increase of mechanical milling times. This is because of the fact that beyond the maximum coercivity point, further mechanical milling results in an amorphous formation which tends to decrease the coercivity considerably in a trend.

It is also seen that the hysteresis loops have a kink or a sharp change of curvature, which indicates a 2-phase formation, in our case the 2-14-1 phase and the α-Fe phase.

Range of coercivities of the $Nd_{12}Fe_{82}B_6$ is always better than the $Nd_{10}Fe_{84}B_6$ because from the phase diagram we understand that there is always greater α-Fe formed for the $Nd_{10}Fe_{84}B_6$. Since α-Fe is the soft phase, this contributes to a lesser coercivity value.

Also it is observed that the range of coercivities is higher for the samples prepared at 10m/s than at 20m/s. The rate of wheel speed and hence the cooling rate is responsible for this. Very fast cooling rates (20m/s) result in not a very good crystalline formation, which results in slightly lesser range of coercivities.

4.1.4 XRD of Annealed data:

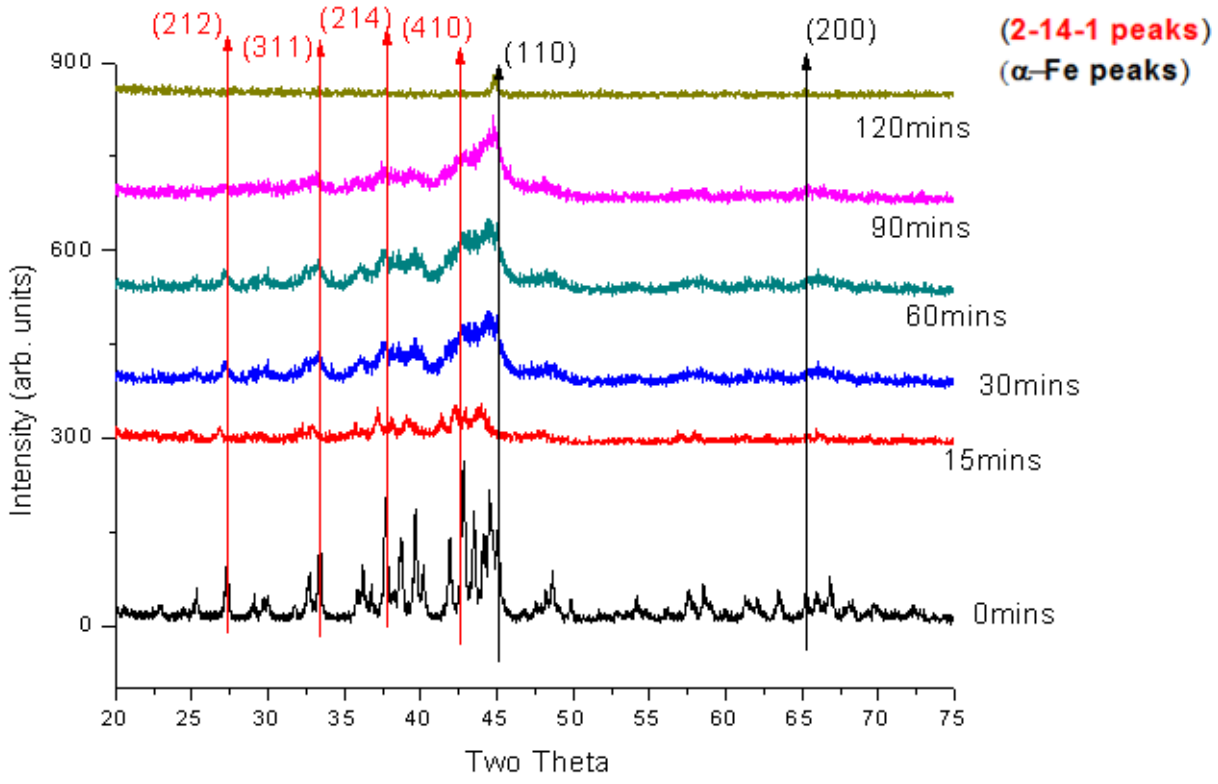

Figure 4.12: *This represent the peaks obtained after annealing each milled sample at 700C for 15minutes, for the $Nd_{12}Fe_{82}B_6$ sample, melt spun at 10m/s.*

Figure represents the XRD of the annealed data for the samples milled for the respective time periods. Certain important observations can be made from these graphs. Firstly it is noticed that

there is not much change in the peak relative intensities and the peak widths for the 0 minutes, 15 minutes and 30 minutes. This is because in these stages of milling, the sample is sufficiently crystalline and therefore there is no further noticeable grain refinement that takes place. However, for the samples that were milled for longer intervals i.e. 60 and 90 minutes, it is noticed that the there is an improvement in the sharpness of the peaks from with respect to their as milled condition. This suggests a phenomenon of grain refinement and improvement in the crystallinity with the heat treatment process.

However for the sample that was milled for 120 minutes, there is no considerable change from the as milled stage in terms of its crystallinity. This can be reasoned by the fact that the temperature that I was doing the annealing was not sufficient enough for it to induce sufficient crystallinity so that it could be seen in the XRD peaks. It had attained a greater degree of amorphous nature and perhaps annealing at a higher temperature would be beneficial in this situation.

4.1.5 Magnetic Measurement of Annealed data: Optimum hysteresis loops indicate how the annealed data compare with the as milled data for optimum values.

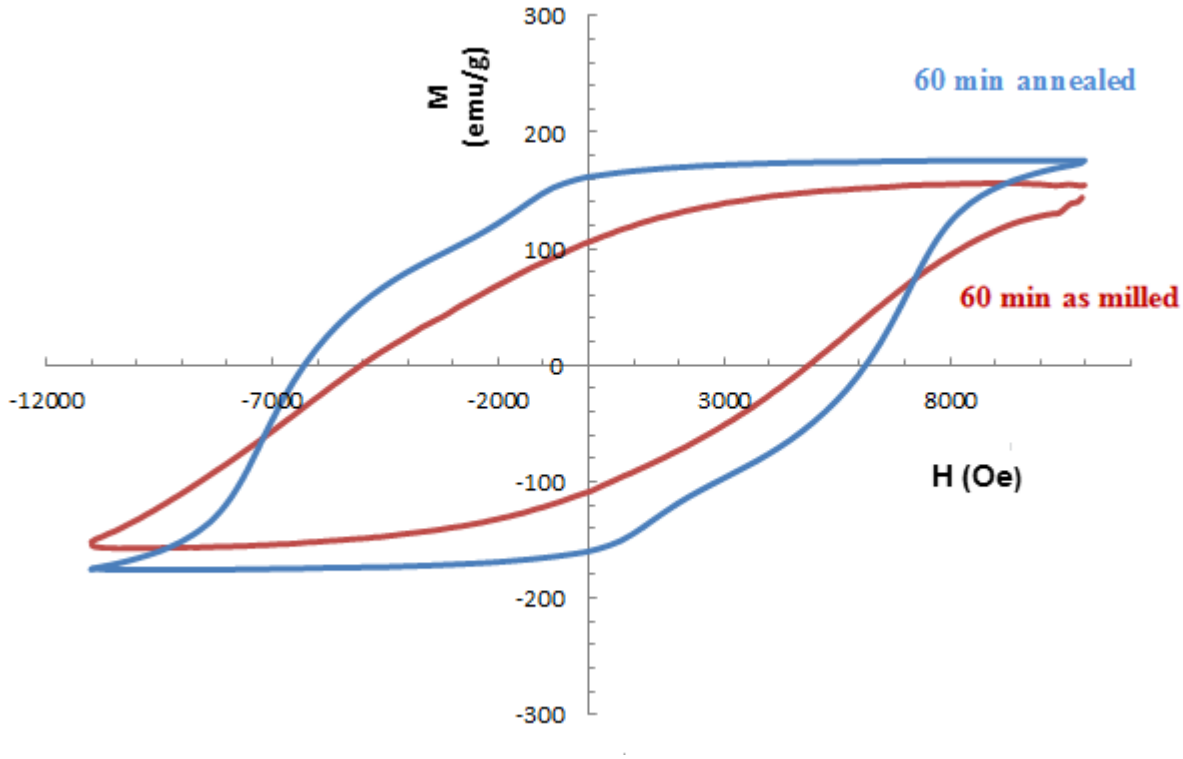

Figure 4.13: *These figures represent the comparison of the optimum hysteresis loops of the* $Nd_{12}Fe_{82}B_6$ *sample, melt spun at 10m/s, and then milled for 60 minutes. The annealing was done at 700C for 15 minutes.*

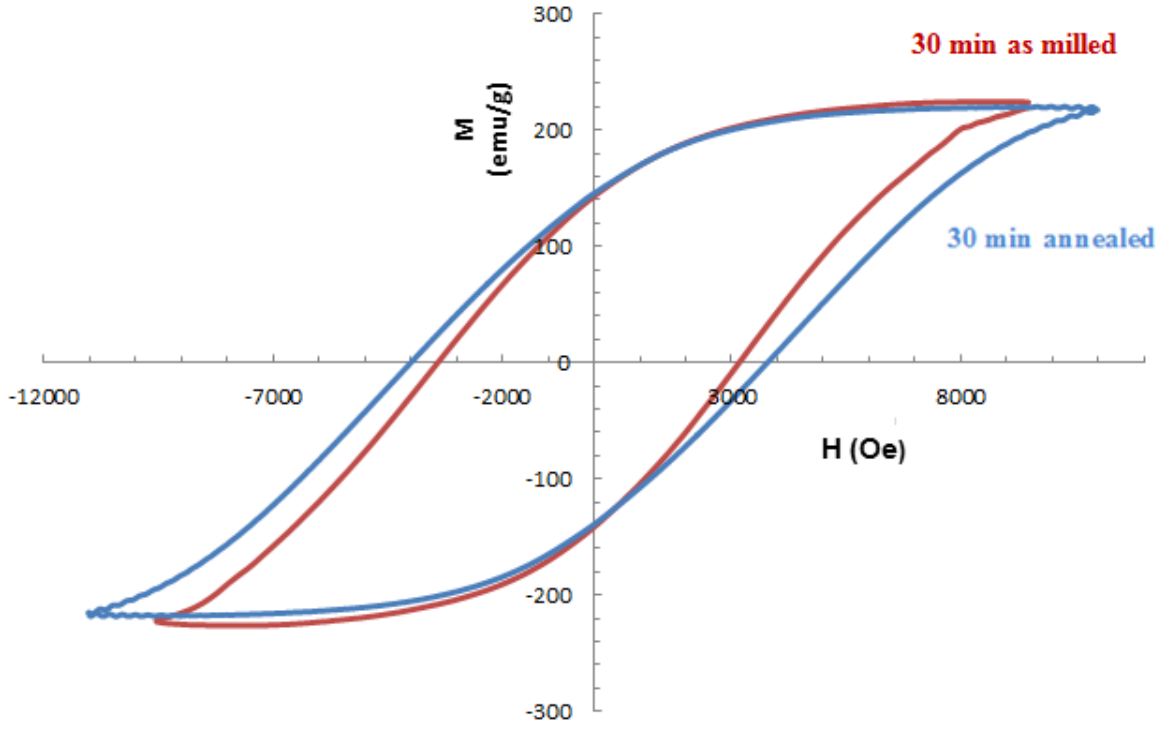

Figure 4.14: *This figure represents the comparison of the optimum hysteresis loops of the* $Nd_{10}Fe_{84}B_6$ *sample, melts spun at 10m/s, and then milled for 30 minutes. The annealing was done at 700C for 15 minutes.*

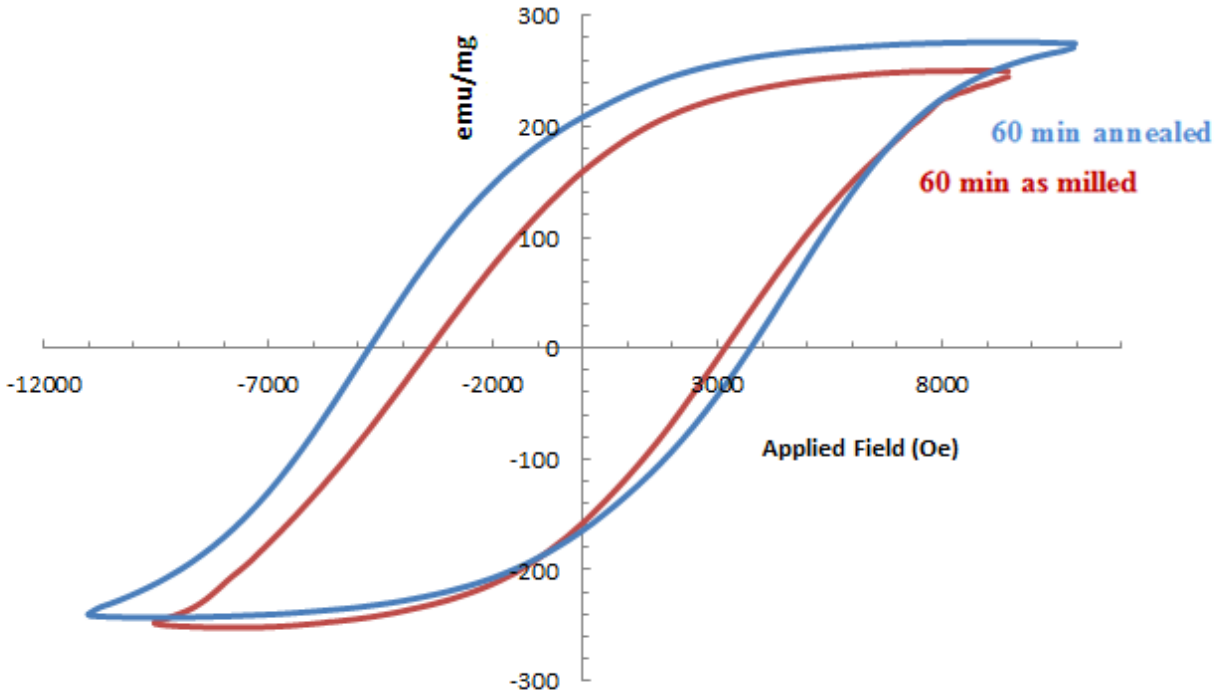

Figure 4.15: *This figure represents the comparison of the optimum hysteresis loops of the* $Nd_{12}Fe_{82}B_6$ *sample, melts spun at 20m/s, and then milled for 60 minutes. The annealing was done at 700C for 15 minutes*

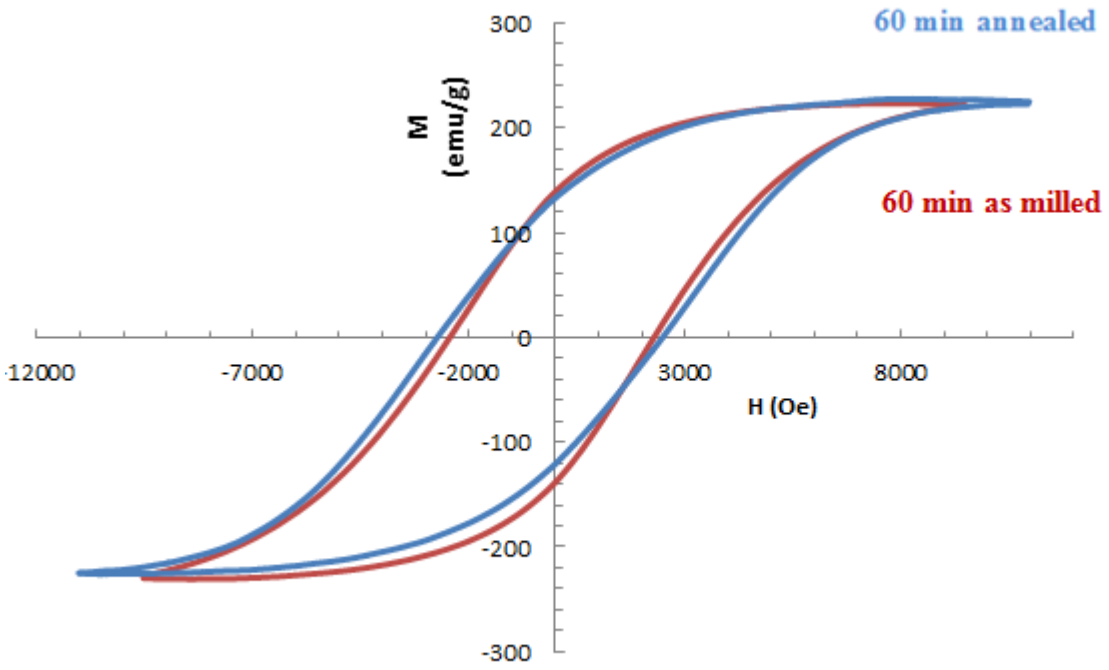

Figure 4.16: *This figure represents the comparison of the optimum hysteresis loops of the $Nd_{10}Fe_{84}B_6$ sample, melts spun at 20m/s, and then milled for 60 minutes. The annealing was done at 700C for 15 minutes*

The figures represent the comparison of the optimum hysteresis loops of the samples and their corresponding annealed counterparts. There is also the graphical representation of as-milled coercivity trend with the trend of annealed coercivities. The annealing was done at 700C for 15 minutes for every sample considered. From the comparison of the data of the optimum hysteresis loops of the as milled and the annealed samples we find some important observations.

Firstly, it is noticed that there is a trend of increasing coercivity in the annealed case as against their as milled counterparts. This can be attributed to the fact that the heat treatment process results in grain refining and improvement in the crystalline order from their amorphous nature. Heat treatment provides the energy necessary for the diffusion of the atoms. Also the heat treatment helps to reduce the stresses introduced in the sample due to the mechanical milling process.

Secondly, the sharp curvatures in some of the hysteresis loops indicate the presence of 2 phases.

4.2 MnIr-Fe SYSTEM – The first stage was the alloying of the Mn with Ir. For this purpose, 3.5g of Iridium and 1.0034g was taken as described above.

4.2.1 Formation of MnIr - MnIr was obtained after annealing the arc melted sample at 700C for 3 days. The graphs are provided as under.

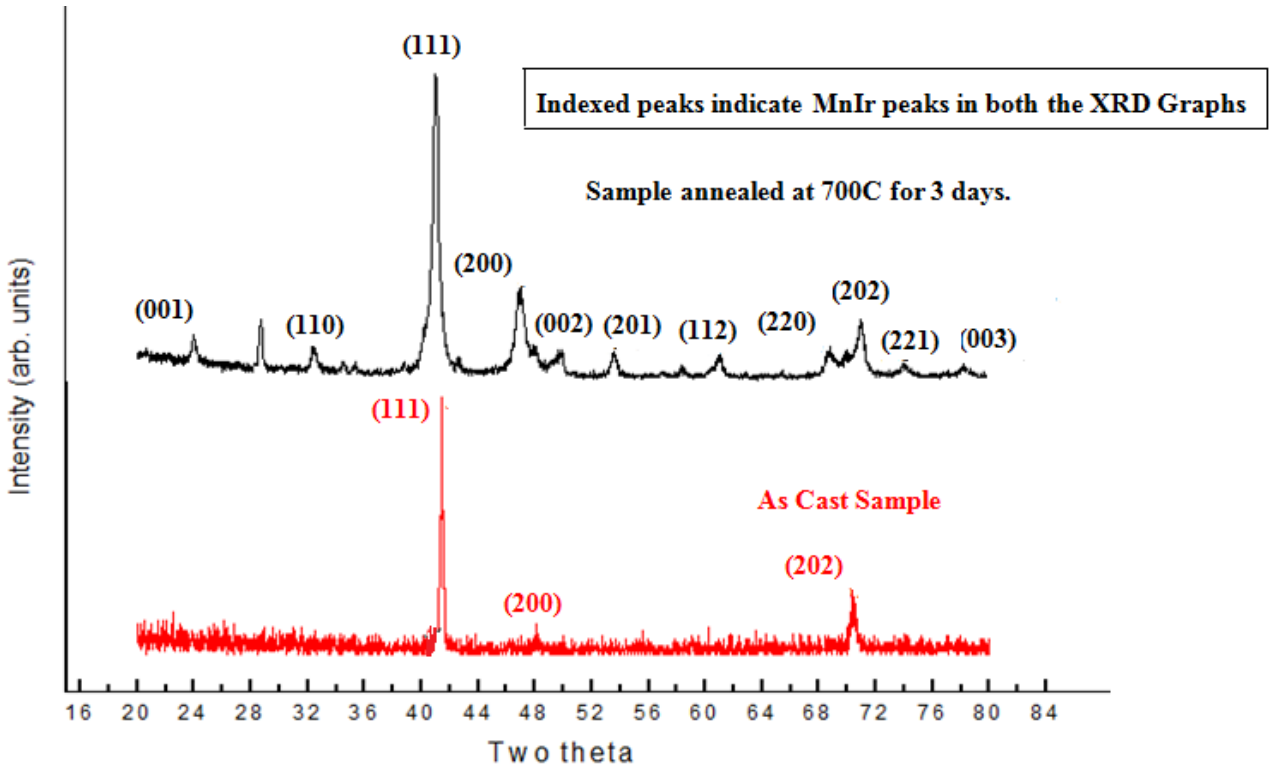

Figure 4.17: *This represents the XRD graphs of the as cast MnIr sample and the sample annealed at 700C for 3 days.*

Figure 4.17 represents the phases obtained for the MnIr alloy that was made by arc melting. The XRD graph at the bottom in red represents the indexed peaks of the MnIr in the as cast condition, whereas the one on the top represents the XRD data of the MnIr after it was annealed at 700C for 3 days. Also very sharp peak formation was detected.

Therefore this can understood by the fact the proper phase was not formed in the as cast condition. However the annealing provided the necessary energy for the diffusion of the atoms to take place and the proper phase to be formed. It helped to form a better crystalline structure, which accounts for the sharpness of the peaks. It can be seen here that almost all the peaks of the MnIr was

obtained and indexed after the annealing. This indicates a very good phase formation due to the heat treatment process.

4.2.2 Alloying with Fe – We add equiatomic amounts of Fe powder to the MnIr ingot which has also been powdered and start ball milling for increasing time intervals. The XRD graphs obtained are given as below:

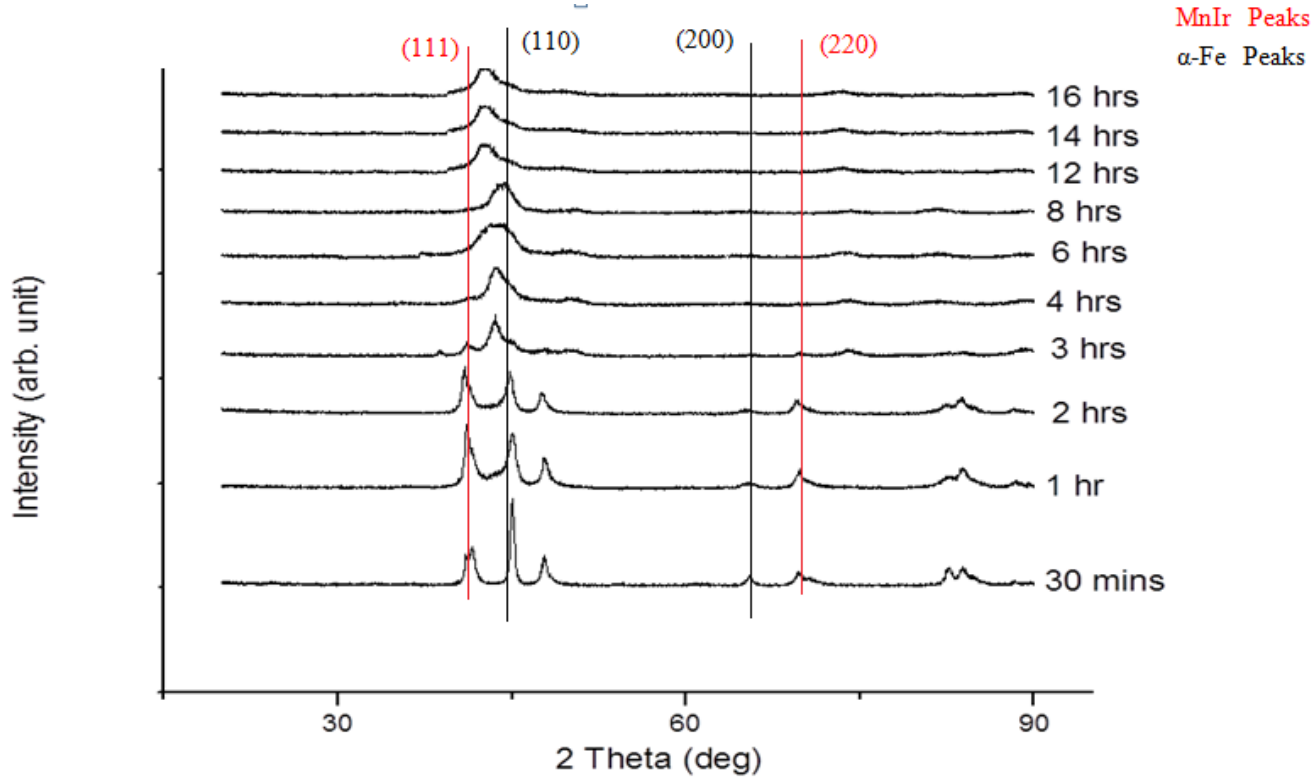

The above graphs indicate that with progressively increasing time intervals, there is a gradual decline of crystallinity, especially at long times of about 16 hours. The continuous beating of the hardened steel balls on the grains causes this condition to take place.

4.2.3 Magnetic Measurements – The magnetic measurements were done with the AGFM and they are represented as under in hysteresis curves.

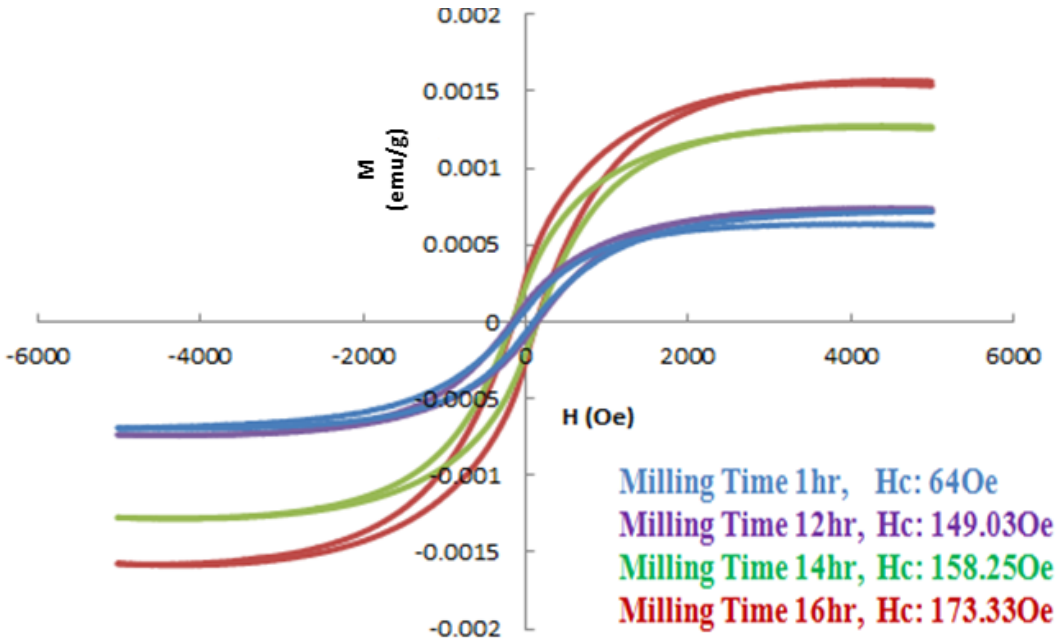

Figure 4.19: *This represents the hysteresis loops of the as milled sample for progressively increasing time intervals.*

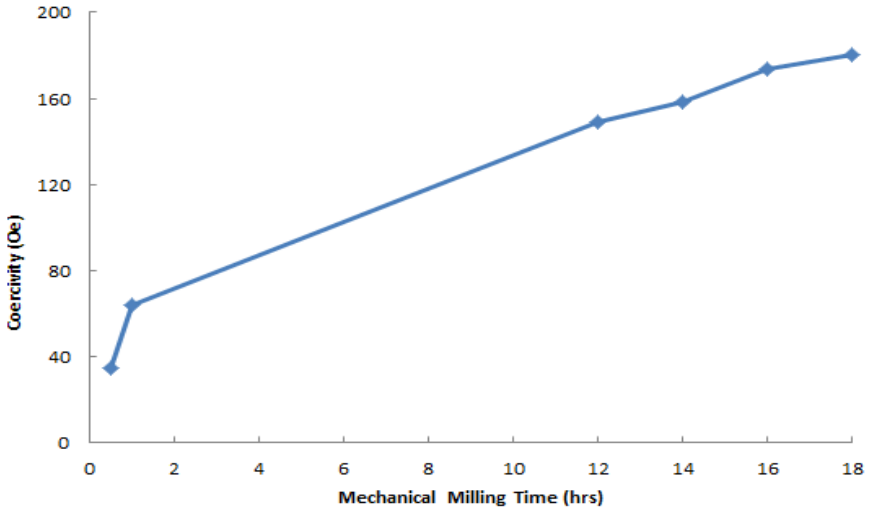

Figure 4.20: *This represents the trend of increasing coercivity with progressively increasing milling times.*

From these hysteresis loops and the graphical representation of coercivity versus milling time, we see that the coercivity shows a slow increase with increase in ball milling times. Also there is a steady increase in the magnetization values. This can be attributed to the fact that with increasing ball milling times, a steady decrease in grain size takes place which improves the coercivity. It is also noticed that there is a trend of increasing remanent magnetization values. This can also be attributed to the exchange interactions occurring due to intimate mixture of the grains at the interface introduced by mechanical milling.

4.2.4 Annealing and Subsequent Magnetic Measurements – After annealing the samples at 700C for 15 minutes, once again magnetic measurements were done. The hysteresis loops are given, in comparison with the non-annealed hysteresis loops for the same ball milled time intervals.

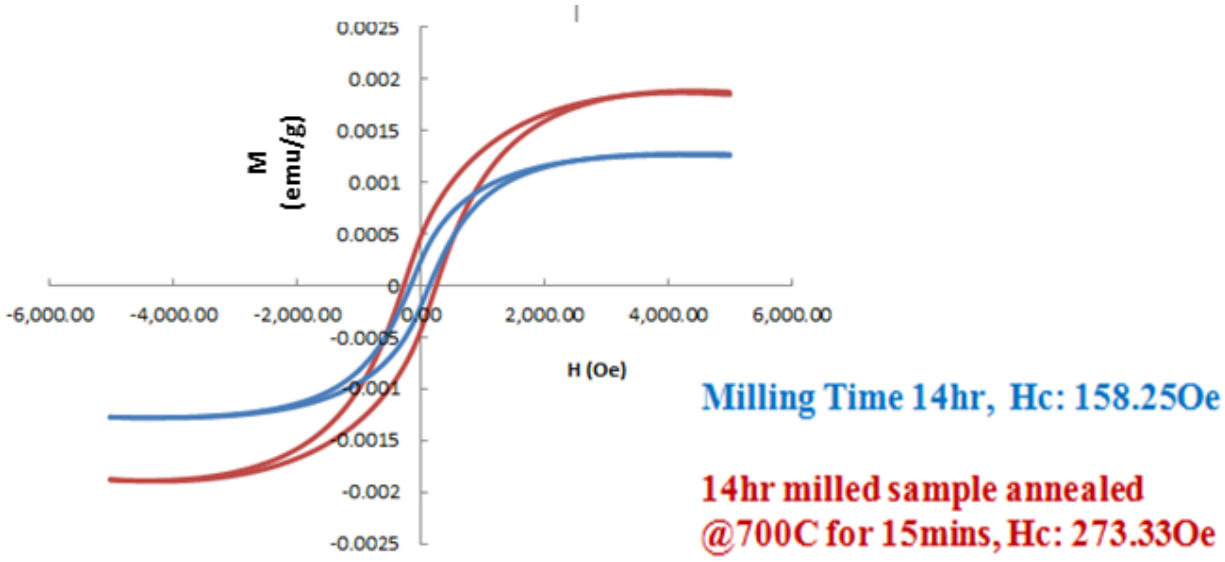

Figure 4.21: *This represents the hysteresis loops of the as milled sample for 14 hours and the same sample annealed at 700 C for 15 minutes.*

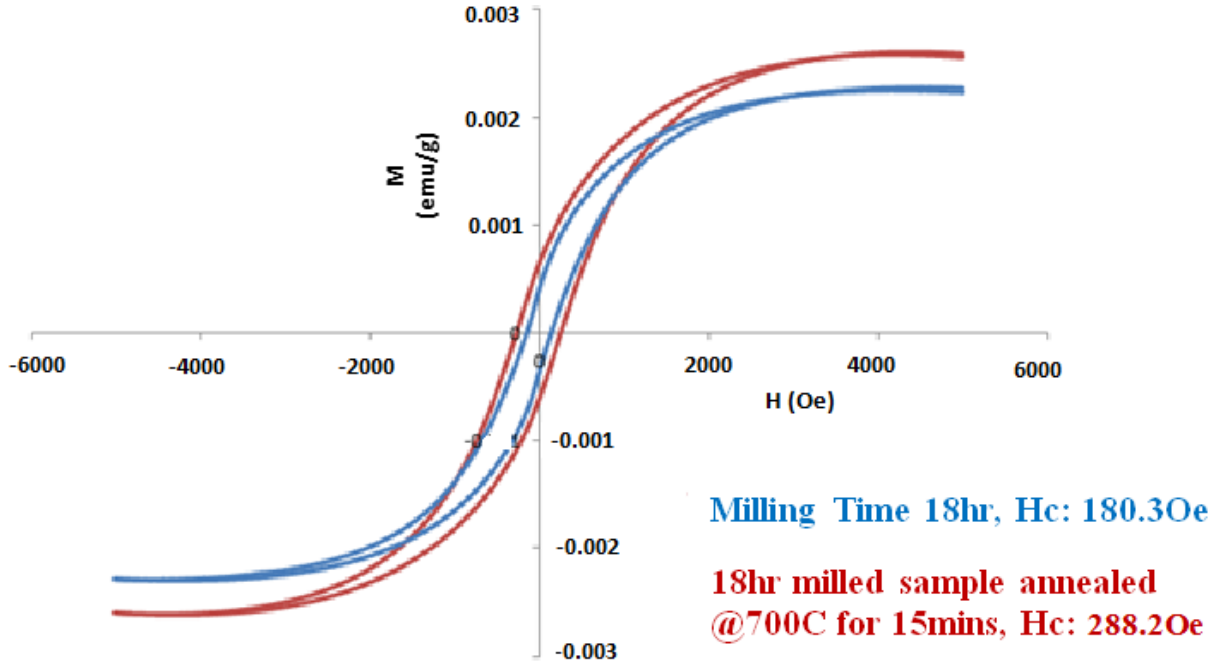

Figure 4.22: *This represents the hysteresis loops of the as milled sample for 18 hours and the same sample annealed at 700 C for 15 minutes.*

The above figure shows the increase in magnetization as well as coercivity of the 14 hour milled sample, both non-annealed (in blue) as well as the annealed sample (in red). The increase in coercivity and magnetization both can be attributed to the grain refinement and formation of crystallites.

The above hysteresis loops show the net improvement in coercivity as well as magnetization for the sample milled for 14 hours and 18 hours, at 700C for 15 minutes. This graph is also similar to the previous showing a trend of increasing coercivity.

This can be also attributed to the fact that there is formation and refinement of crystallites with annealing. Annealing provides the necessary energy for the diffusion of the atoms to improve the

crystalline nature of the sample. These two factors tend to have a synergistic effect in improving the net magnetic parameters (coercivity and remanent magnetization).

4.2.5 X-Ray of Annealed Samples: The X-Ray Data of the annealed samples can be represented as under.

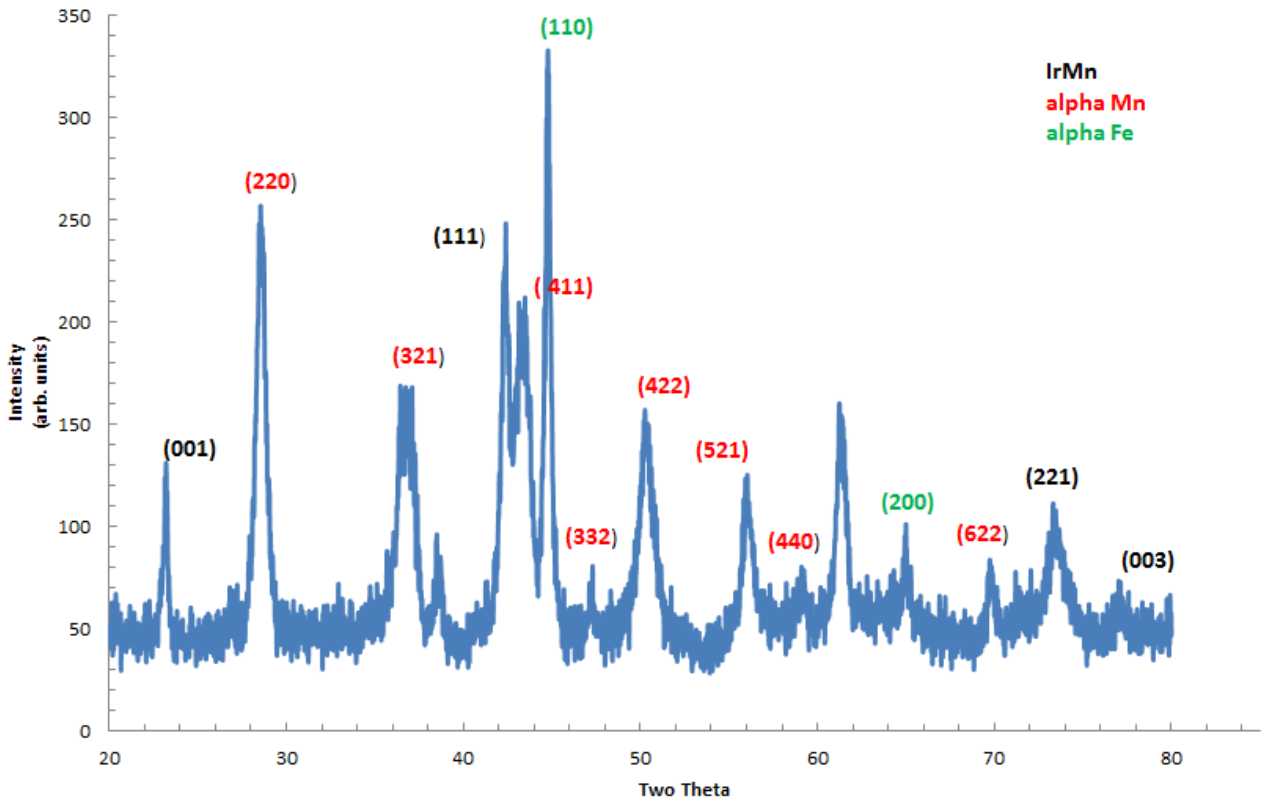

Figure 4.23: *XRD Graphs of the phases present in the sample that was milled for 14, after being annealed at 700C for 15 minutes. The color codes for the various phases obtained are shown in the inset.*

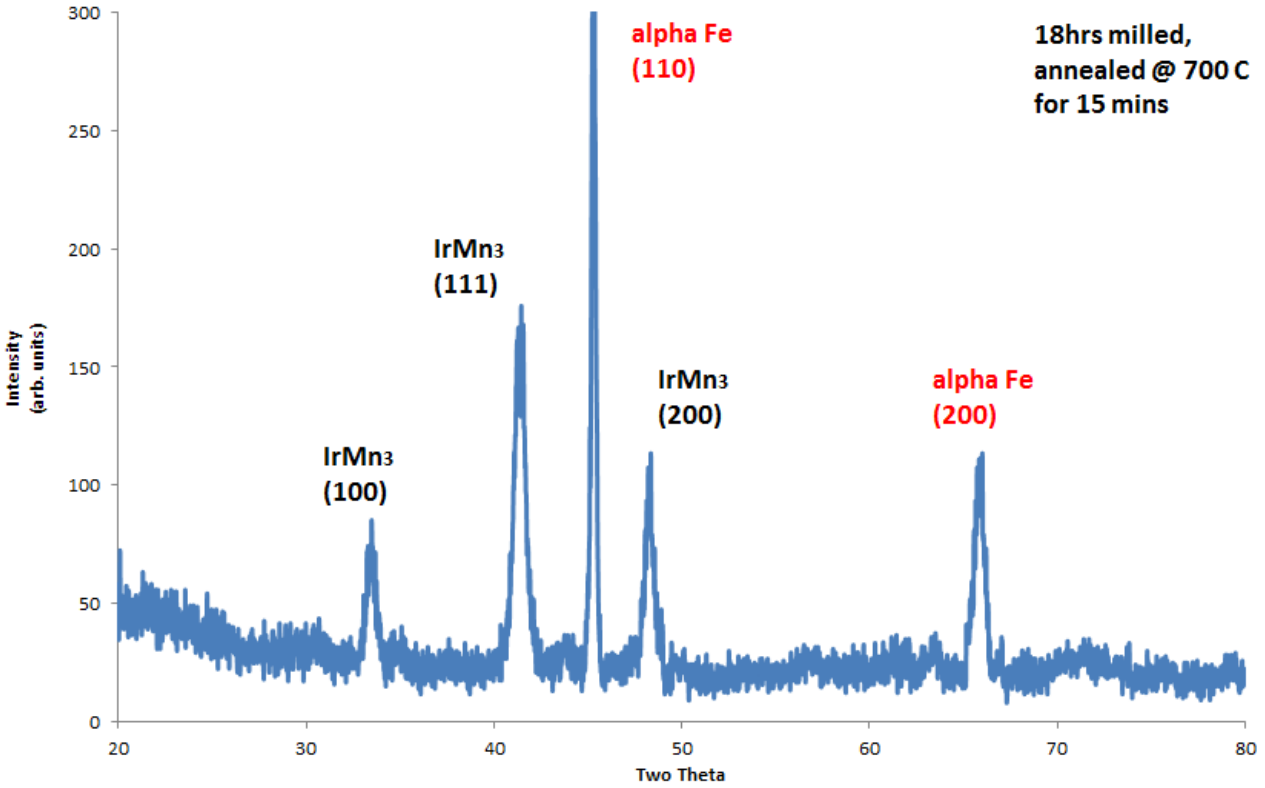

Figure 4.24: *These represent XRD Graphs of the phases present in the sample that was milled for 18 hours, after being annealed at 700C for 15 minutes. Again the color codes for the various phases obtained are shown in the inset.*

The XRD data of the annealed samples shows us the phases that are obtained. As is seen, we get some alpha-Fe along with equiatomic IrMn along with other phases. Grain refinement due to annealing (heat treatment) can be attributed to the formation of these phases.

5. CONCLUSION

Permanent magnets are ubiquitous materials which have a wide variety of applications from car motors to applications as storage medium in hard disk drives in computers. Also rare earth metals, which act as important components in permanent magnets are getting more costly and scarce. Therefore my thesis is an effort in that direction to improve the properties of permanent magnets at a lesser cost by reducing the usage of rare earth metals.

The effect of cooling speed and heat treatment on the microstructure and magnetic properties of the alloys have been studied. For the Nd-Fe-B system it has been understood that the cooling rates, i.e. the wheel speeds have an important effect of the microstructure. Also the effect of annealing tends to provide improved coercivity. Two different compositions have been studied by varying the milling times both before and after annealing. It has been seen that coercivity tends to improve the coercivity upto a point beyond which it decreases because of the amorphous nature introduced due to longer milling times.

For the MnIr-Fe system, I have tried to utilize the principle of exchange interaction and also heat treatment to obtain good paramagnetic properties. No previous studies have been done on the MnIr-Fe system and there is still a lot of scope for improvement in this system which can be done with introducing other alloying elements to improve coercivity. Longer milling times and different annealing conditions can also be studied to look for improvements in coercivity and overall magnetic properties.

6. REFERENCES

1. B.D. Cullity, *Introduction to Magnetic Materials*, IEEE Press, Second Edition.

2. Charles Kittel, *Introduction to Solid State Physics*, Wiley Press, India, Seventh Edition.

3. William D. Callister Jr. and David G. Rethwisch, *An Introduction to Materials Science and Engineering,* Wiley Press, Eighth Edition.

4. M. Tisza, *Physical Metallurgy for Engineers*, ASM International and Freund Publishing House Ltd., Ohio, 2000.

5. V. Raghavan, *Materials Science and Engineering*, Prentice Hall of India Private Limited, Fifth Edition, 2005.

6. Laughlin, David E., Srinivasan, K., Tanase, M. and Wang, L., *Crystallographic aspects of $L1_0$ magnetic materials*, Scripta Materialia, **53**, 383-388, (2005).

7. Skomski, R., Kashyap, A. and Zhou, J., *Atomic and micromagnetic aspects of $L1_0$ magnetism*, Scripta Materialia, **53**, 389-394, (2005).

8. Yamaoka, T., *Antiferromagnetism in ¥-phase MnIr alloys*, Journal of the Physical Society of Japan, **Vol. 36, No. 2**, (1974).

9. http://en.wikipedia.org/wiki/Exchange_interaction

10. Kneller, E.F. and R. Hawig, R., *The exchange spring magnet: a new material principle for permanent magnets*, IEEE Transactions, **Vol. 27, Issue 4**, 3588 – 3560, (1991).

11. Coehoorn, R. De Mooij, D.B., Duchateau, J.P.W.B. and Buschow, K.H.J., *Novel Permanent Magnetic Materials Made by Rapid Quenching*, Journal De Physique, **C8-669**, (1988).

12. Hadjipanayis, George C. *Nanophase hard magnets*, Journal of Magnetism and Magnetic Materials, **Volume 200, Issues 1-3**, 373 – 391, (1999).

13. Gao, R.W., et al. *Exchange-coupling interaction, effective anisotropy and coercivity in nanocomposite permanent materials*, Journal of Applied Physics, **94**, 664-668, (2003).

14. Talijan, N., Stajic-Trosic, J., Grujic, A., Cosovic, V., Menushenkov, V., Aleksic, R., *Nanocomposite Permanent Magnetic Materials Nd-Fe-B type/The Influence of Nanocomposite on Magnetic Properties*, Journal of Mining and Metallurgy, **41B**, 95-102, (2005).

15. Sagawa, M., Fujimura, S., Yamamoto, H., Matsuura, Y., *Permanent Magnet Materials Based on Rare Earth-Iron-Boron-Tetragonal Compounds,* IEEE Transactions on Magnetics, **Vol. 20**, 1584-1589, (1987).

16. Erde, W., and Lianxi, H., *Nanocrystalline and Ultrafine Grained Materials by Mechanical Alloying,* Trans Tech Publications, Switzerland, 534-536, (2009).

17. Miao, W.F., Ding, J., McCormick, P.G. and Street, R., *A comparative study of mechanically alloyed and mechanically milled* $Nd_{10}Fe_{84}B_6$, Journal of Applied Physics, **79**, (1996).

18. Nogues, J., Sort, J., Langlais, V., Doppiu, S., Dieny, B., Munoz, J.S., Surinach, S., and Baro, M.D., *Exchange bias in ferromagnetic nanoparticles embedded in an antiferromagnetic matrix*, Int. J. Nanotechnology, **Vol. 2**, (2005).

19. McCusker, L.B., Von Dreele, R.B., Cox, D.E., Louer D. and Scardi, P., *Rietveld refinement Guidelines, Journal of Applied Crystallography*, **32**, 36 – 50, (1999).

20. De Castro, Claudio L. and Mitchell, Brian S., *Nanoparticles from Mechanical Attrition*, Tulane University.